

Steps towards a solution of the FS Aurigae puzzle – II. Confirmation of the intermediate polar status

V. V. Neustroev^{1*}, G. H. Tovmassian², S. V. Zharikov², and George Sjöberg^{3,4}

¹*Astronomy Division, Department of Physics, PO Box 3000, FIN-90014 University of Oulu, Finland*

²*Instituto de Astronomia, Universidad Nacional Autonoma de Mexico, Apdo. Postal 877, Ensenada, Baja California, 22800 Mexico*

³*The George-Elma Observatory, Mayhill, New Mexico, USA*

⁴*American Association of Variable Star Observers, 49 Bay State Road, Cambridge, MA 02138, USA*

Accepted 2013 April 10. Received 2013 March 15; in original form 2012 August 8

ABSTRACT

FS Aur is famous for a variety of uncommon and puzzling periodic photometric and spectroscopic variabilities. It was previously proposed that the precession of a fast-rotating magnetically accreting white dwarf can successfully explain these phenomena. We present a study of FS Aur based on two extensive sets of optical photometric observations and three X-ray data sets in which we intended to verify whether the observational properties of the long period modulations observed in FS Aur and V455 And are similar in appearance to the spin modulation in ordinary IPs. These new optical observations have revealed, for the first time in photometric data, the variability with the presumed precession period of the white dwarf, previously seen only spectroscopically. We also found that the modulations with the precession and orbital periods are evident in X-ray data. We show that the observed properties of FS Aur closely resemble those of other intermediate polars, thus confirming this cataclysmic variable as a member of the class.

Our analysis of multicolour observations of intermediate polars has shown that time-series analysis of colour indices appears to be a powerful technique for revealing hidden variabilities and shedding light on their nature. We have found that the $(B - I)$ power spectrum of V1223 Sgr indicates the presence in the data of the spin pulsation which is not seen in the optical light curve at all. Also, the analysis of the colour indices of V455 And revealed the presence of the photometric variations which, similarly to FS Aur, was previously observed only spectroscopically.

Key words: binaries: close – novae, cataclysmic variables – X-rays: stars – stars: white dwarfs – stars: individual (FS Aurigae, V455 Andromedae, V1223 Sagittarii)

1 INTRODUCTION

Cataclysmic Variables (CVs) are close interacting binary stars which consist of a white dwarf (WD) accreting material from a Roche-lobe-filling companion, usually a late main-sequence star. Intermediate polars (IP) are an important subset of CVs in which the magnetic field of the WD is strong enough to disrupt the inner accretion disc or even prevent disc formation completely and to force the accreting material to flow along field lines onto one or both magnetic poles.

CVs are known to be very active photometrically, showing variability on time scales from seconds to years (see review by Warner 1995). However, the only strictly periodic system clocks in CVs are associated with the binary orbital period and the rotation of the WD. They may also produce modulation sidebands (beat

periods) often observed in light curves of IPs (see Warner 1986 for the origin of optical pulsations in CVs). In addition to these strictly periodic oscillations, unstable quasi-periodic oscillations and superhumps may appear in the light curves of CVs. We note that all these variabilities have periods much shorter, equal, or very close to the orbital period of the binary system.

FS Aurigae represents one of the most unusual CV to have ever been observed. The system is famous for a variety of uncommon and puzzling periodic photometric and spectroscopic variabilities which do not fit well into any of the established subclasses of CVs. FS Aur was discovered by Hoffmeister (1949), who classified it as a dwarf nova. $H\alpha$ velocity variations with a period of 85.7 min ascribed to the binary orbital period (OP), have been reported by Thorstensen et al. (1996). This period was confirmed by follow-up spectroscopic observations (Neustroev 2002; Tovmassian et al. 2003; Tovmassian, Zharikov, & Neustroev

* E-mail: vitality@neustroev.net

2007). Neustroev (2002) also detected substantial orbital variability of emission line profiles and their equivalent widths.

The light curve of FS Aur is highly variable in its appearance, only sometimes showing the OP. The outlandish peculiarity of FS Aur is the existence of well-defined photometric optical modulations with the amplitude of up to ~ 0.5 mag and a very coherent long photometric period (LPP) of 205.5 min that exceeds the OP by 2.4 times (Neustroev 2002; Tovmassian et al. 2003). Furthermore, in late 2004 the optical brightness of the system dropped by 2 magnitudes for a few months. The spectral observations made in December 2004, revealed a second long spectroscopic period (LSP) of 147 minutes, appearing in the far wings of the emission lines. Frequency of this new period is equal exactly to the beat between the OP and LPP: $1/P_{beat} = 1/P_{orb} - 1/P_{phot}$ (Tovmassian, Zharikov, & Neustroev 2007). It is interesting to note that the LPP has never been detected spectroscopically whereas the LSP has not been seen in the photometric data.

The photometric and spectroscopic behaviour of FS Aur somewhat resembles that of IPs in which several periodic signals are often observed. Nevertheless, the principal difference between FS Aur and IPs is in the time-scales of their variabilities: (a) most IPs are relatively long orbital period systems: only 5 of the 36 confirmed/ironclad IPs¹ have an OP below the period gap, and probably one more system lies in the period gap;

(b) a spin period of WD in all IPs is shorter than the orbital one, typically $P_{spin} \leq 0.1P_{orb}$ (for a detailed review on IPs, we refer the reader to Patterson 1994 and Hellier 1996). In contrast, the period which is proposed to be the OP of FS Aur, is the shortest of all the detected periods in the system, and is only a little longer than in SDSS J233325.92+152222.1 – the IP with the shortest-known orbital period.

This fact may call into question whether the orbital period has been correctly identified in FS Aur, and why, for instance, are 205.5m, 147m and 85.7m not the orbital, beat and spin periods, respectively? None the less, we claim that the 85.7 m period is indeed the OP and our arguments are the following:

(i) It is commonly accepted that radial velocities are a much more reliable indicator of the orbital period than photometric variability. The LPP is the only period of the three detected in FS Aur which is not seen spectroscopically, and as such can be definitely ruled out as an orbital period.

(ii) Both the 85.7 m period and the LSP are observed spectroscopically. The emission lines in many IPs also vary at the orbital and spin periods. In few cases, emission-line fluxes, equivalent widths and radial velocity variations with the spin period dominate over variations with the orbital period. We note, however, that the character of these two types of variabilities is very different. The profiles of broad emission lines found in most of CVs are generally determined by the macroscopic motion of the emitting gas in the binary system. The periodic motion, due to Doppler shifts, generates spectral components with a sinusoidal modulation of wavelength which revealed themselves as coherent S-waves in a trailed spectrogram. Participating in the orbital motion, the main contributors to the emission lines – the accretion disc, secondary star, gas stream and bright spot – superpose many such S-waves with a wide range of velocity amplitudes and create a characteristic multicomponent trailed spectrogram. A good collection of such spectrograms is provided by Honeycutt, Schlegel, & Kaitchuck (1987).

The trailed spectra of FS Aur folded with the 85.7 m period closely resemble many of them. In contrast, the sources of the spin spectral variability are located in a more compact area around the accretion curtain and/or the innermost part of the accretion disc and as such dominate in the far wings of emission lines (Hellier 1999). The LSP variability in FS Aur has much more similarities with such spin variability. Thus, we have no reason to believe that the LSP is the true orbital period, instead of the 85.7 m one.

(iii) In V455 And, another cataclysmic variable which, similarly to FS Aur, exhibits two very different spectral periods – a short one of 81 min and a longer one of 210 min (Tovmassian, Zharikov, & Neustroev 2007) – eclipses in the system’s light curve unambiguously confirms the OP to be 81 minutes.

We therefore conclude that the weight of evidence favours 85.7 m as the OP of FS Aur. The nature of the two other periods is thus still an open question. Neither the LPP nor the LSP can be accepted as the period of rotation of the WD. On theoretical grounds, the spin period of the WD in IPs is determined by the combined action of accretion and magnetic field (Norton, Wynn, & Somerscales 2004). Fast rotation can be expected given the large amount of angular momentum transferred by accreting matter. The WD is expected to spin-up to a value near to the rotation period at the inner edge of the accretion disc (King & Lasota 1991; Warner & Wickramasinghe 1991). From the observational point of view, no CVs have been found with the primary rotating so slowly.

Thus, the discovered multiple periodic phenomena in FS Aur represent a real challenge to the theory of accretion processes in low mass close binaries. Moreover, several other systems are now known to show variabilities with periods much longer than the orbital one (GW Lib, V455 And), and the origin of these modulations also remains unclear. It seems that FS Aur and similar objects can represent a new type of CVs, which still needs an explanation of their nature.

In order to explain the puzzling behaviour of FS Aur, Tovmassian et al. (2003) proposed, and Tovmassian, Zharikov, & Neustroev (2007) enhanced the IP scenario with a fast-rotating, magnetically accreting WD which precesses with the LSP (see Section 3.2 in Tovmassian, Zharikov, & Neustroev 2007). Due to the magnetic nature of the WD, the accreting material in FS Aur should be controlled and channelled by the strong magnetic field of the WD within its magnetospheric radius, as it is in an ordinary IP. However, as the WD is involved in two periodic motions – rotational and precessional – one could expect to observe stable modulations in the optical and X-ray light curves with both the periods. Observational properties of these modulations should depend, among other things, on geometrical factors such as the angles between the magnetic, rotational and precessional axes, but they should both be similar in appearance to the spin modulation in IPs.

The search for a WD spin modulation in FS Aur is still to be concluded. The first attempt to detect this modulation was made by Neustroev et al. (2005). Even though they found a signature of ~ 101 and/or 105 sec oscillation in the optical power spectra, there is still no conclusive evidence.

It appears that FS Aur may have even longer photometric period, which was described and discussed by Chavez et al. (2012). A dynamical solution for that very long photometric period (VLPP) may have an influence on the stochastic variability, but most likely

¹ The catalog of IPs and IP candidates (Version 2011a) by Koji Mukai, <http://asd.gsfc.nasa.gov/Koji.Mukai/iphome/catalog/alpha.html>

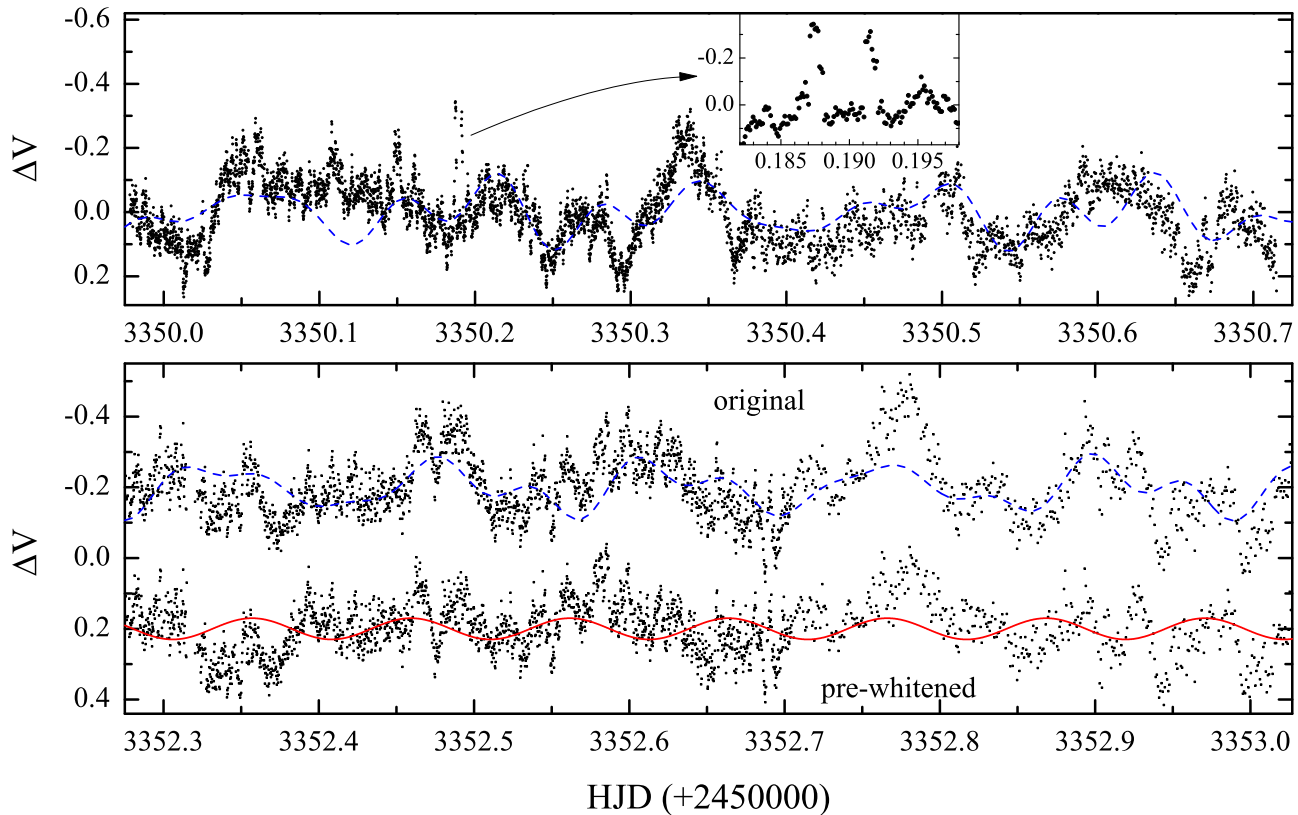


Figure 1. Two 18 hour samples of the V light curve of FS Aur from *set-04*. In the inset of the upper panel two half-magnitude flares with durations shorter than 100 sec are shown. In the lower panel the original light curve (upper) is shown along with the light curve (bottom) pre-whitened by the LPP frequency and its first harmonic and by the OP frequency. The dashed blue lines are the sum of sinusoidal fits of the LPP and its first harmonic and the OP which yielded the ephemeris (2) and (1). The solid red line is a fit of the LSP corresponding to the ephemeris (4).

is not directly related to the shorter, strictly periodic variabilities discussed in this paper.

In this paper, we present the analysis of two extensive sets of optical photometric observations and three X-ray data sets of FS Aur. We also present the analysis of optical multicolour photometric observations of V455 And. We intended to verify whether the observational properties of the long period modulations observed in FS Aur and V455 And are similar in appearance to the spin modulation in ordinary IPs. We compared our results with the multicolour observations of eight ironclad and confirmed IPs, generously provided to us by our colleagues worldwide. For one more well-known IP V1223 Sgr, we used our own multicolour observations.

2 OBSERVATIONS

2.1 Optical observations

2.1.1 The 2004 multi-site observational campaign

In late 2004, in order to obtain a long uninterrupted light curve of FS Aur, we acquired optical time-series photometry with the broadband Johnson–Cousins filter V using three telescopes located in South Korea, Italy and Mexico. In South Korea, the observations were made using the SITE 2048 \times 2048 CCD camera attached to the $f/8$ Cassegrain focus of the Bohyunsan Optical Astronomy Ob-

servatory (BOAO) 1.8 m telescope. In Italy, the observations were obtained using the imaging spectrograph BFOSC with a 1300 \times 1340 pixels EEV CCD attached to the Cassini 1.5 m telescope at Loiano. In Mexico, the observations were performed at the Observatorio Astronómico Nacional (OAN SPM) on the 1.5-m telescope using the SITE S1003 CCD camera. A part of the latter observations were obtained simultaneously with the spectroscopic observations presented in Tovmassian, Zharikov, & Neustroev (2007) and which we analyze in this paper again. Unfortunately, due to not-optimal weather conditions we were unable to obtain any whole-day observations. We did acquire four long observations with a duration of 16–18 hours each. Selected comparison and check stars from the field were used for differential photometry performed using the standard reduction systems MIDAS and IRAF. Two 18 hour samples of this light curve are shown in Figure 1.

Additional photometry was acquired by members of the Center for Backyard Astrophysics (CBA)². For details of their activity and procedures used to obtain and reduce the data, we refer to Patterson (2011).

Hereinafter we call this set of observations *set-2004*. Table 1 provides a journal of these observations.

During this observational campaign, FS Aur was found to exhibit a decrease in luminosity of 2 mags that lasted a few months until the end of 2005 January (Tovmassian, Zharikov, & Neustroev

² See <http://cba.phys.columbia.edu>

Table 2. Journal of photometric observations of FS Aur (set-2011).

HJD start 2450000+	Duration (hours)	Band	Comments	HJD start 2450000+	Duration (hours)	Band	Comments	HJD start 2450000+	Duration (hours)	Band	Comments
5536.611	10.00	V	Outburst	5575.564	9.09	V		5621.586	5.80	BVRI	
5537.608	10.02	V	Outburst	5576.651	6.96	V		5622.667	3.61	BVRI	
5538.606	10.00	V		5577.565	2.58	V		5623.590	5.64	BVRI	Outburst
5539.603	9.99	V		5581.823	1.96	BVRI		5625.591	4.44	BVRI	Outburst
5541.610	10.16	V		5582.568	6.07	BVRI		5626.588	5.15	BVRI	Outburst
5542.596	10.66	V		5583.571	8.64	BVRI		5629.589	5.07	BVRI	
5543.593	10.61	V		5584.570	5.05	BVRI		5648.660	2.10	BVRI	Outburst
5544.591	10.67	V		5587.583	8.11	BVRI	Outburst	5649.598	3.20	BVRI	
5545.588	10.64	V		5588.596	7.65	BVRI		5650.598	3.62	BVRI	
5548.715	7.61	V		5589.572	8.45	BVRI		5651.601	3.25	BVRI	
5551.703	5.12	V	Outburst	5590.572	8.46	BVRI		5652.601	3.86	BVRI	
5552.595	9.94	V	Outburst	5591.572	8.32	BVRI		5654.631	2.68	BVRI	
5554.591	9.28	V		5596.592	7.37	BVRI		5865.708	7.33	BVRI	
5555.566	9.81	V		5597.576	6.48	BVRI		5866.705	7.58	BVRI	
5556.557	10.78	V		5598.576	7.39	BVRI	Outburst	5867.701	4.68	BVRI	
5557.578	10.61	V		5600.575	3.10	BVRI	Outburst	5868.698	7.41	BVRI	
5559.597	9.81	V		5603.579	7.08	BVRI		5870.695	7.78	BVRI	Outburst
5562.727	6.79	V		5604.608	6.44	BVRI		5871.712	7.26	BVRI	Outburst
5563.656	7.97	V		5605.579	5.85	BVRI		5872.688	7.91	BVRI	Outburst
5564.557	10.82	V		5607.581	6.93	BVRI	Outburst	5873.687	8.04	BVRI	
5565.557	10.28	V	Outburst	5608.606	4.92	BVRI		5874.682	5.02	BVRI	
5566.589	9.22	V	Outburst	5609.720	3.17	BVRI		5875.680	7.96	BVRI	
5567.558	9.58	V	Outburst	5610.638	4.43	BVRI		5892.679	8.39	BVRI	
5569.558	8.81	V		5612.606	4.22	BVRI		5894.637	9.50	BVRI	
5570.561	10.20	V		5613.603	1.74	BVRI		5895.633	9.55	BVRI	Outburst
5571.560	3.98	V		5614.584	6.57	BVRI		5896.629	9.50	BVRI	Outburst
5573.561	7.71	V		5615.584	6.31	BVRI		5899.632	9.64	BVRI	
5574.609	8.09	V		5616.585	6.31	BVRI		5913.581	10.09	BVRI	Outburst

2007). As the character of the variability of the star has changed somewhat during the campaign (see below), we divide these data into two subsets. Observations taken between HJD 2453347–2453358 we call *set-04*, the rest of the data taken between HJD 2453383–2453406 we call *set-05*.

2.1.2 The 2010-2011 observational campaign

During the winter of 2010-2011 we initiated and conducted an observing campaign, lasting more than 150 consecutive nights. During this campaign we observed 11 consecutive low-amplitude outbursts (≤ 2 mag) (Neustroev et al. 2012). The bulk of these data will be discussed elsewhere. Here we mostly concentrate on observations obtained in the quiescent state.

The data presented in this paper were taken using the 0.35-m Celestron C14 robotic telescope, located at New Mexico Skies in Mayhill, New Mexico. Before the night of February 24, we used an SBIG ST-8XME CCD camera with 1530×1020 pixels, and since then it was replaced with an SBIG ST-10XME, 2184×1472 pixels. Both cameras were used with Johnson-Cousins $BV(RI)_C$ Astrodon Photometrics filters.

The observations were conducted every clear night from November 26, 2010 until May 3, 2011. Thus, more than 80 nights of time-resolved photometry were taken (38 of them were in quiescence), and almost 14 000 V -band data points were obtained. Additionally, between January 20 and March 9, 2011, 31 nights of time-resolved multicolor $BV(RI)_C$ photometry were taken (22 of them were in quiescence). Moreover, after acceptance of our Swift ToO request (see below), we obtained 5 more nights of multicolour

observations (3 nights were in quiescence), between March 28 and April 3, 2011. Depending on the weather conditions, we monitored the star for 6–8 hours per night in the beginning of the campaign and for 3–4 hours in the end.

The following autumn we continued monitoring FS Aur. Between the nights of October 31 and December 4, 2011, 15 nights of time-resolved multicolour photometry were taken (8 nights were in quiescence).

During all quiescent observations, exposure times were 240 seconds for the VRI filters and 400 seconds for B . The observations were taken quasi-simultaneously in the $V B V R I$ sequence. The reduction procedure was performed using the IRAF environment and the software AIP4Win v. 2.4.0 (Berry & Burnell 2005). All of the FS Aur photometry used the secondary standards found in Henden & Honeycutt (1997) to establish the zero points. Henden & Honeycutt (1997) do not provide R magnitudes, so instead we used R magnitudes from Misselt (1996). The typical accuracy of our measurements varied between 0.01 and 0.10 mag depending on the brightness of the object and the weather conditions. The median value of the photometric errors in the quiescent state was 0.03 mag in the VRI filters and 0.04 mag in B .

Hereinafter we call this set of observations *set-2011*. Table 2 provides a journal of this set of observations.

2.2 X-ray data

From previous X-ray observations we know that FS Aur is a rather hard and relatively bright X-ray source with a count-rate of 0.13 counts/s as observed with *ROSAT* PSPC (Tovmassian et al. 2003),

Table 1. Journal of photometric observations of FS Aur (*set-2004*). The horizontal line divides two subsets, *set-04* and *set-05*.

HJD start 2450000+	Duration (hours)	Exp. Time sec.	Band	Telescope*
3347.010	8.69	10	V	BOAO
3347.691	16.54	10	V	SPM-BOAO
3348.676	15.89	10	V	SPM-BOAO
3349.978	17.69	5, 10	V	BOAO-Loiano
3350.984	17.78	5, 10	V	BOAO-Loiano
3351.719	7.37	60	white	CBA
3352.275	10.30	10	V	Loiano
3352.682	8.27	60	white	CBA
3353.659	8.82	60	white	CBA
3354.671	8.52	60	white	CBA
3355.652	8.97	60	white	CBA
3356.661	8.52	60	white	CBA
3358.681	8.06	60	white	CBA
<hr/>				
3383.615	7.85	60	white	CBA
3388.635	6.88	60	white	CBA
3390.633	6.92	60	white	CBA
3394.620	6.72	60	white	CBA
3403.589	6.96	60	white	CBA
3404.624	6.13	60	white	CBA
3405.631	5.96	60	white	CBA
3406.612	6.40	60	white	CBA

* Telescopes:

BOAO – Bohyunsan Optical Astronomy Observatory, South Korea
 CBA – Center of Backyard Astronomy
 Loiano – Osservatorio Astronomico di Bologna, Stazione di Loiano, Italy
 SPM – Osservatorio Astronomico Nacional San Pedro Martir, Mexico

Table 3. Log of the *Chandra* and *Swift* observations of FS Aur.

Observatory Dataset	ObsId	Obs. date	HJD start 2450000+	Exp. (sec)
Chandra	5189	2005-01-05	3375.612	25180
Swift-2007	00030873001	2007-01-17	4117.921	6690
	00030873002	2007-01-18	4118.525	11797
	00030873003	2007-01-19	4119.528	10693
Swift-2011	00030873004	2011-03-29	5650.304	4055
	00030873005	2011-03-30	5651.034	3934
	00030873006	2011-03-31	5652.237	4323
	00030873007	2011-03-31	5652.509	8148

suggesting that the system might be an IP. Most IPs show modulations at the spin and orbital periods. Motivated by our findings, described in the following Section, we have found that it is instructive to compare the optical and X-ray light curves of FS Aur. A log of the X-ray observations is presented in Table 3.

The *Chandra* ACIS-S observations of FS Aur which were performed on January 5, 2005 with a total on-source exposure of 25 ksec, allow a direct comparison with our optical *set-2004*. These data were analyzed following the standard procedures using CIAO³ (Version 4.3) provided by the *Chandra* X-ray Center (CXC).

During the 2010-2011 observational campaign, we also performed a ToO observation of FS Aur with the X-ray telescope

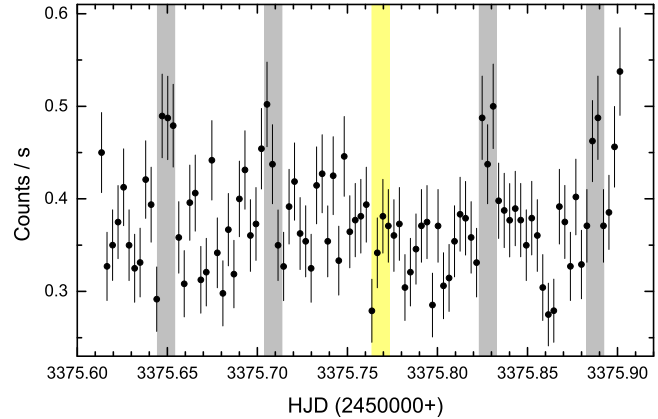


Figure 2. The X-ray light curve of FS Aur obtained with *Chandra* and binned at 264 s intervals. The shaded areas are centered on the orbital phase interval 0.27–0.43 during which strong and narrow periodic flares were observed. One of these peaks (marked by yellow area instead of grey) was seen to be missing.

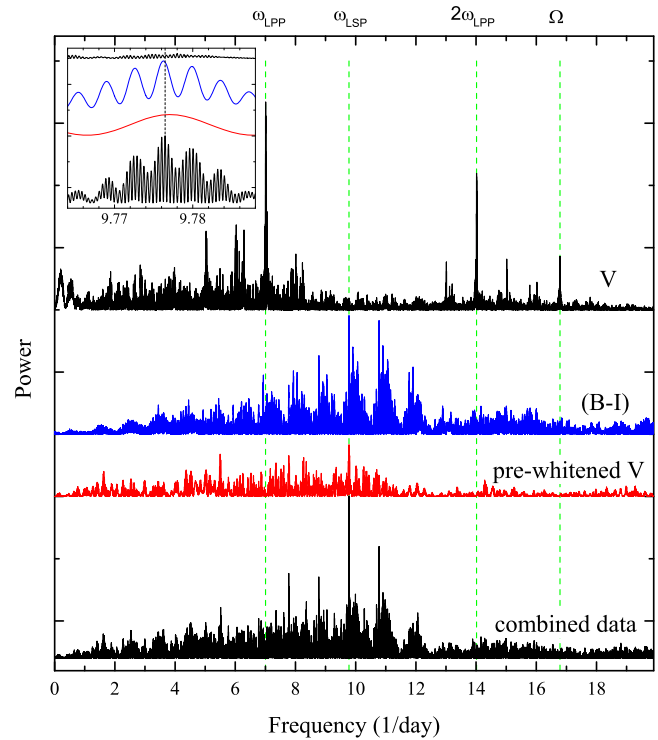


Figure 3. The Lomb-Scargle power spectra for different sets of optical data of FS Aur. The upper black line represent the spectrum for the entire V photometry. The strongest peaks at $f = 7.0077 \text{ day}^{-1}$ and 14.0161 day^{-1} correspond to the LPP and its first harmonic. Another relatively strong peak at 16.7848 day^{-1} corresponds to the orbital frequency. The three bottom spectra were calculated from the $(B - I)$ colour-index data from the *set-2011* (blue), from the pre-whitened V light curve from the *set-2004* (red), and from the combined data set consisting of the former two and the ULTRACAM colour data (black, see Section 3.3 for details). The strongest peaks in these spectra at $f = 9.77644 \text{ day}^{-1}$ exactly coincide with the LSP which is the presumed precession period of the WD. The inset shows the enlarged region around the LSP frequency.

³ <http://cxc.harvard.edu/ciao/>

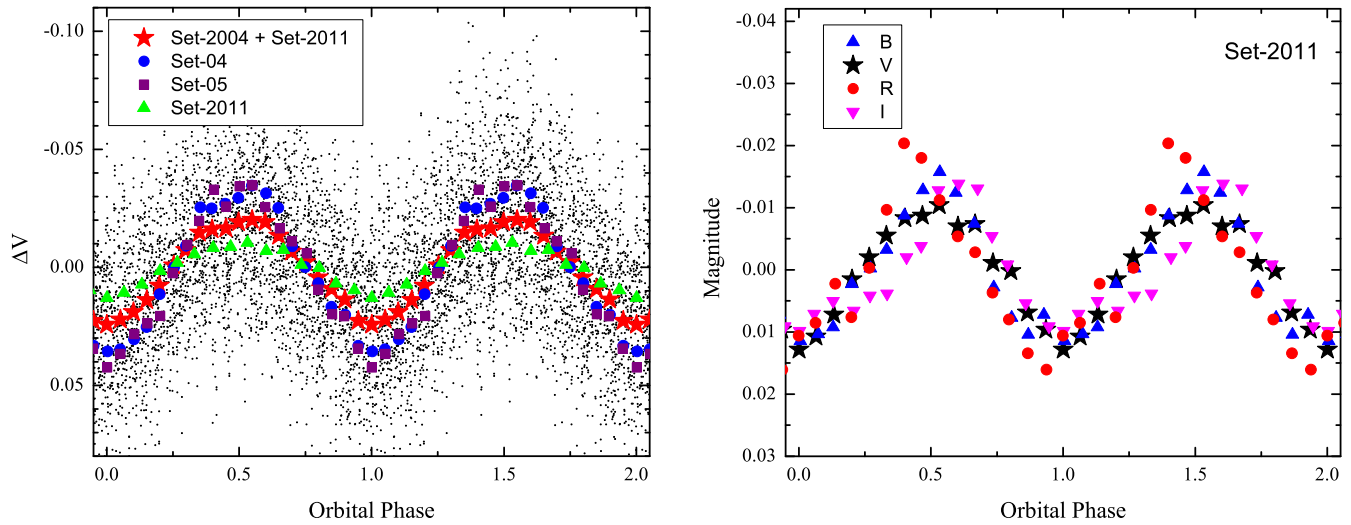


Figure 4. *Left:* the entire pre-whitened V phase curve (with the means, and linear trends subtracted for each night of observations) folded with the OP according to the ephemeris (1). The large symbols represent data from different subsets averaged in 20 phase bins. *Right:* the folded light curves in different colours of the *set-2011*. All data are plotted twice for continuity.

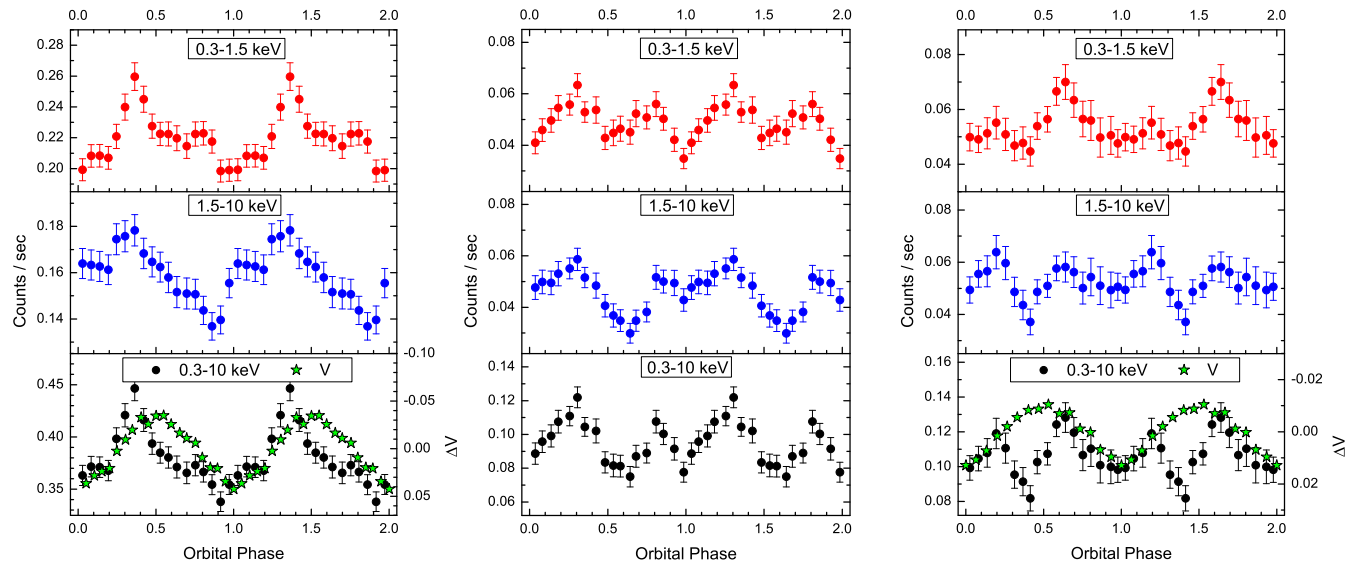


Figure 5. The Chandra (left panel), Swift-2007 (middle) and Swift-2011 (right) data folded with the OP according to ephemeris (1). The panels are from top to bottom: the soft range (0.3-1.5 keV), hard range (1.5-10 keV), and the total X-ray flux (0.3-10 keV). The latter are shown together with the corresponding V light curves (the Chandra data are compared with the optical *set-05* whereas the Swift-2011 is compared with the *set-2011*). Two cycles are shown for continuity.

(XRT) and the UV-Optical Telescope (UVOT) onboard the Swift X-ray satellite (Gehrels et al. 2004). These observations were taken on March 29 – April 1, 2011 for a total of about 20.4 ksec. The object was also observed by Swift on another occasion during January 17 – 19, 2007 with a total on-source exposure of 30 ksec. Hereinafter we call these sets of observations “Swift-2011” and “Swift-2007”. We used the Swift Release 3.7 software⁴ together with the most recent version of the Calibration Database to analyze the Swift data. The XRT data were reduced in the standard fashion with `xrtpipeline` (v. 0.12.6). In 2007, the UVOT observations in the

`uvw2` and `uvm2` filters were taken in event mode. These data were used for evaluation of the short-term variability. They were reduced following the procedure described in Poole et al. (2008).

In order to analyze the X-ray variability with the fundamental periods, we extracted soft (0.3-1.5 keV) and hard (1.5-10 keV) light curves. For the spectral analysis, the background-subtracted spectra in the energy range 0.3-10 keV were extracted and averaged for each dataset.

⁴ <http://swift.gsfc.nasa.gov/docs/software/lheasoft/>

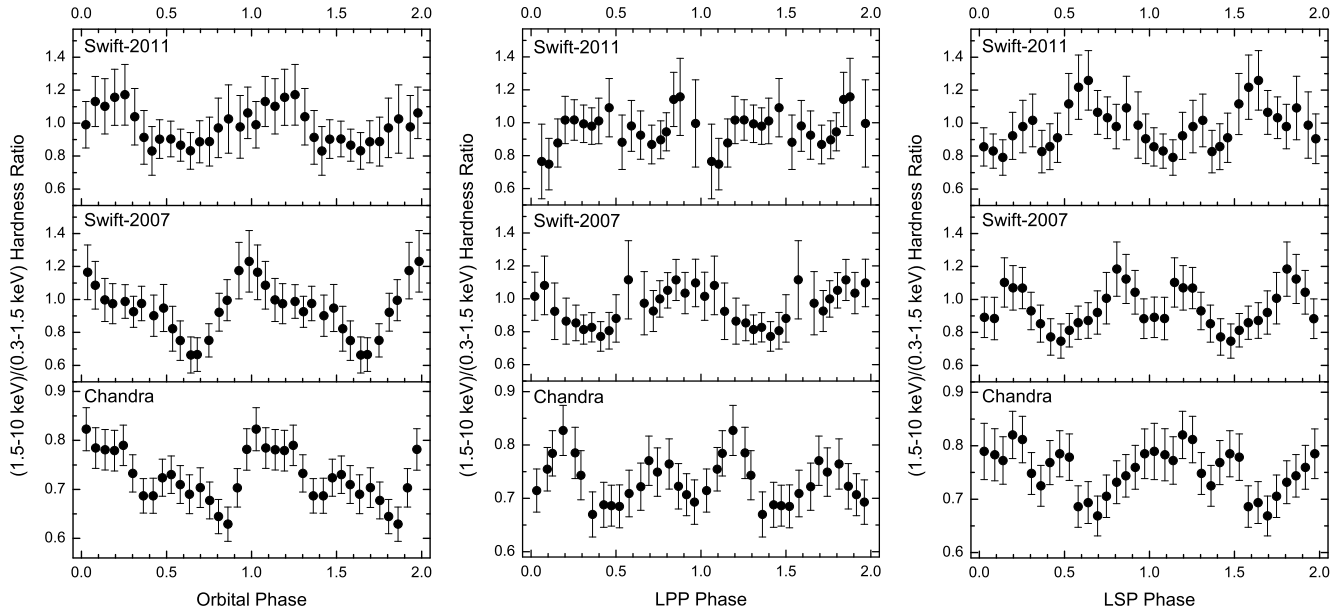


Figure 6. Hardness ratio curves of FS Aur folded with the OP (left panel), the LPP (middle) and the LSP (right) according to the ephemerides (1), (2) and (4), respectively.

3 DATA ANALYSIS

It has been previously shown that usually the most prominent features of the optical light curve of FS Aur is the well-defined LPP modulation of 205.5 min contaminated by strong stochastic variations (Neustroev 2002; Tovmassian et al. 2003; Neustroev et al. 2005). The orbital variability was previously seen only occasionally while the LSP variability was never observed photometrically. However, during the presented observations the photometric behavior of FS Aur was significantly different yet consistent across both sets of the data. In particular, the character of the LPP variability was changed, the OP modulation was apparent most of the time, the LSP variability was observed in colour curves, and stochastic variations were exceptionally strong.

The Lomb-Scargle periodogram for the entire V photometry (with the means, and linear trends subtracted for each night) is shown in Figure 3. Comparing this power spectrum with the one presented in Figure 6 of Tovmassian et al. (2003), one can also find apparent differences: the strongest, very sharp peak at $f = 7.0077 \pm 0.0001 \text{ day}^{-1}$ related to the LPP is now accompanied by its first harmonic at $f = 14.0161 \pm 0.0001 \text{ day}^{-1}$ which was not observed previously, and the appearance of the relatively strong peak at the orbital frequency $f = 16.7848 \pm 0.0001 \text{ day}^{-1}$.

The relative shortness of the X-ray observations obviously does not allow us to perform a time series analysis. We note, however, that the most prominent feature of the Chandra light curve is the modulation with the OP that can be seen even with the naked eye (Fig. 2). In order to perform a more detailed analysis, we folded the X-ray light curves with the OP, LPP and LSP.

3.1 The orbital variability

In order to analyze the optical OP variability, we first pre-whitened the light curve by the LPP frequency and its first harmonic (see Section 3.2). The entire 7 year set of photometry is of sufficient quality to compute an accurate ephemeris:

$$T_{min} = 2453346.970(2) + 0.05958096(5) \cdot E \quad (1)$$

where the initial epoch is defined as the time of the minimum in the V light curve, as it is more likely to represent inferior conjunction of the donor star in FS Aur. Figure 4 (left panel) shows the entire pre-whitened V light curve folded according to the ephemeris (1) and averaged in 20 phase bins.

Folding different subsets of the data over the OP results in the same smooth and almost perfectly sinusoidal shape of the modulation, yet with slightly different amplitudes. In the right panel of Figure 4 we show the folded light curves in different colours of the *set-2011*. All these light curves have the same shape and amplitude, but the R light curve exhibits some phase shift in comparison with the V one, whereas the B and I light curves are in phase with it. It is not easy to explain such anomalous behaviour of the R light curve. A possible reason might be lower amplitude of the OP modulation during the *set-2011* and relatively high noise level in the corresponding data.

From the radial velocity study of the H α , H β and H γ emission lines conducted in Tovmassian, Zharikov, & Neustroev (2007), we can now compare the relative phasing of the photometric and radial velocity modulations with the OP. Assuming that the emission lines come from disc material orbiting the WD, the red-to-blue crossing of the radial velocities provides an estimate of the moment of inferior conjunction of the secondary star. Using radial velocity measurements made with a double Gaussian separation of 600 km s $^{-1}$ (for details see Tovmassian, Zharikov, & Neustroev 2007), we estimated the moment of inferior conjunction of the secondary star in FS Aur to be HJD 2453346.971 \pm 0.001.

It is well known that measurements of emission-line radial velocities in CVs often give quite uncertain or incorrect results, as the emission lines arising from the disc may suffer several asymmetric distortions. However, almost perfect coincidence between the initial epochs estimated by different methods allows us to consider this moment as inferior conjunction of the secondary star.

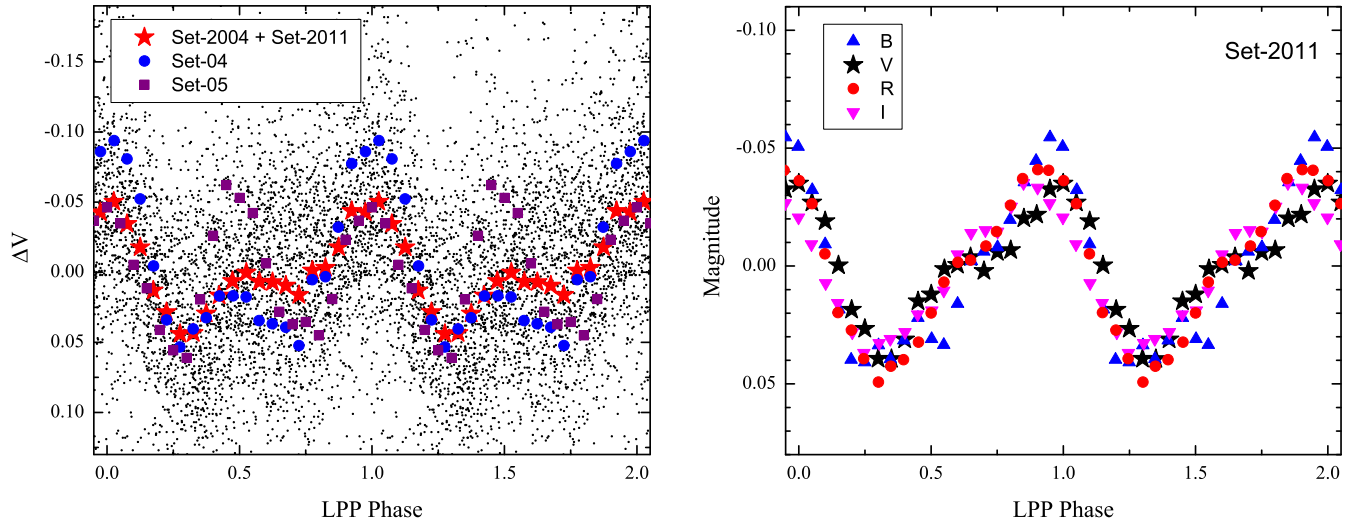


Figure 7. *Left:* the entire V phase curve (with the means, and linear trends subtracted for each night of observations) folded with the LPP according to the ephemeris (2). The large symbols represent data from different subsets averaged in 20 phase bins. *Right:* the folded light curves in different colours of the *set-2011*. All data are plotted twice for continuity.

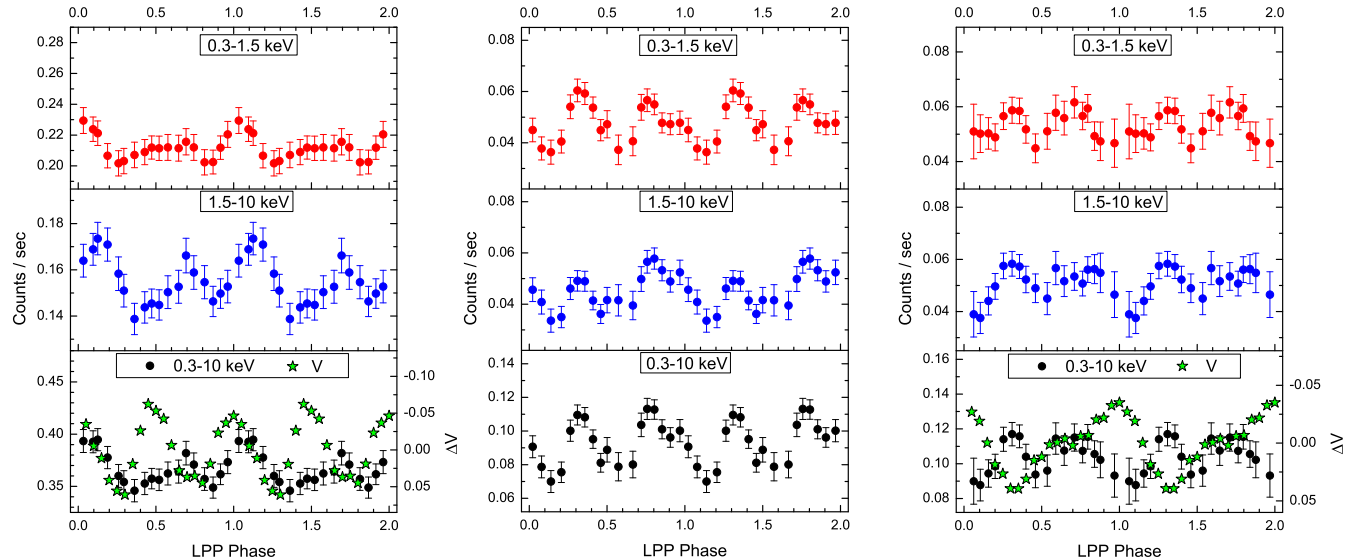


Figure 8. The Chandra (left panel), Swift-2007 (middle) and Swift-2011 (right) data folded with the LPP according to ephemeris (2). The panels are from top to bottom: the soft range (0.3-1.5 keV), hard range (1.5-10 keV), and the total X-ray flux (0.3-10 keV). The latter are shown together with the corresponding V light curves (the Chandra data are compared with the optical *set-05* whereas the Swift-2011 is compared with the *set-2011*). Two cycles are shown for continuity.

In X-rays, the modulation with the OP is also strong in both energy ranges (Fig. 5). However, there are significant differences in the X-ray light curves between different X-ray sets and at different energies as seen from the hardness ratio curves (Fig. 6, left panel). The folded Chandra light curve is quasi-sinusoidal and displays a broad maximum with an additional strong and narrow peak which is visible almost exclusively in the soft band. This peak is so strong that it is evident even in the raw data. Note, that one of these peaks was seen to be missing (Fig. 2).

The Swift light curves display a similar quasi-sinusoidal modulation which is distorted by a broad depression which is deeper in the hard band. The peak maximum in the Chandra data and the depression minimum in the Swift-2011 are observed at nearly same

phase 0.4, whereas in the Swift-2007 the minimum is shifted toward later phases. The sinusoidal component in all the X-ray data sets closely correlates with the optical light curves.

3.2 The LPP variability

From the previous observations of FS Aur it was known that the LPP modulations can be varied in strength and appearance, but on average the light curve was smooth and almost perfectly sinusoidal (see Figures 4 and 7 in Tovmassian et al. 2003). Nevertheless, the new photometric data reveal that the LPP modulation has changed dramatically, being transformed from a sinusoidal shape to a double-hump one. We defined the following accurate ephemeris:

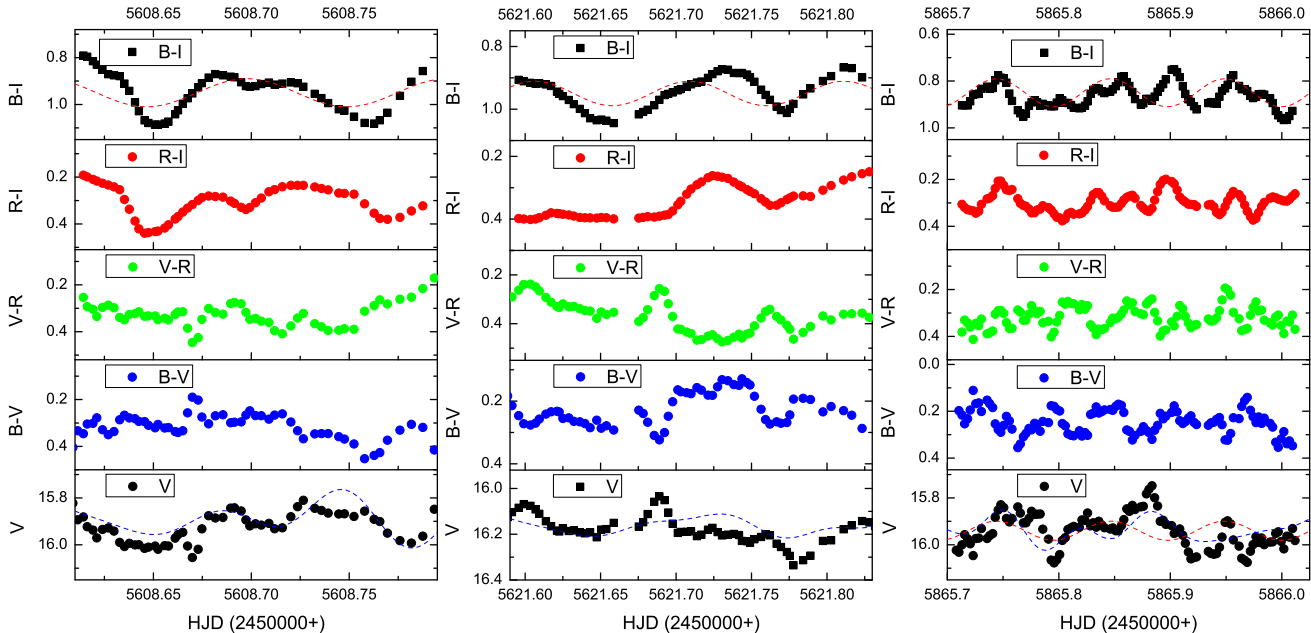


Figure 9. Sample V light curves and $(B - V)$, $(V - R)$, $(R - I)$ and $(B - I)$ colour curves of FS Aur from JD 2455 608, JD 2455 621 and JD 2455 865. The dashed blue lines are the sum of sinusoidal fits of the LPP and its first harmonic and the OP which yielded the ephemeris (2) and (1). The dashed red line is a fit of the LSP corresponding to the ephemeris (4). Note that on the night of JD 2455 865 the LSP modulation is also visible in the V light curve.

$$T_{max} = 2453346.915(2) + 0.14270191(9) \cdot E \quad (2)$$

where the initial epoch is defined as the time of primary maximum in the binned V light curve. Figure 7 (left panel) shows the entire V light curve folded according to this ephemeris and averaged in 20 phase bins.

Folding different subsets of the data over the LPP results in the slightly different morphology of the modulation. Not only the amplitude of the modulation but also the relative strength of the two humps varies substantially between the different subsets. However, despite such dramatic changes from previous observations, the LPP modulation kept an important feature – its amplitude is the same in different colour bands (Figure 7, right panel).

Similar double-hump modulation was also observed in each X-ray set (Fig. 8). The amplitude of variations is about the same in the soft and hard X-ray ranges but there appears to be some energy dependence of this modulation, most prominent in the Chandra data, as seen in the hardness ratio curves (Fig. 6, middle panel).

Despite the similarity in morphology of the modulation profiles, we note a considerable phase shift between optical and X-ray pulses, different in the Chandra and Swift data sets.

3.3 The LSP variability

FS Aur and V455 And compose a group of CVs in which the emission lines vary with two very different periods, namely the OP and LSP. Such a behaviour is very unusual for ordinary dwarf novae but it is common for Intermediate Polars which often show more than one periodicity in the emission lines (Hellier, Cropper, & Mason 1991; Hellier 1999). We note, however, that those additional periods are usually quite clearly seen in optical light curves of IPs, whereas neither in FS Aur nor in V455 And was the LSP ever detected in optical photometry.

At first sight, the presented observations are not an excep-

tion. No significant power is detected at the LSP frequency (~ 9.78 day $^{-1}$) neither in the total power spectrum nor in the periodograms of the subsets (see the inset in Figure 3).

As it was shown before, the optical light curve of FS Aur is dominated by the LPP and OP modulations, which amplitudes are approximately the same in all filters. However, the colour curves $(B - V)$, $(V - R)$ and $(R - I)$ also show a noteworthy variation, more or less following the brightness variation: the colour indices $(B - V)$ and $(R - I)$ are generally in anti-phase and $(V - R)$ is in phase with the light curve (Fig. 9). The amplitudes of colour variations are $\sim 0.1 - 0.2$ mag in all these colours.

Surprisingly, we found that the behavior of the colour index $(B - I)$ is notably different. The most noticeable feature in $(B - I)$ is a modulation with a period near 0.1 day, even though it is sometimes contaminated or even completely replaced by the OP/LPP variations and flickering. After visual inspection of the nightly $(B - I)$ curves, we selected a total of 19 nights (half of the observations taken in quiescence) when this variability is most evident. The Lomb-Scargle periodogram of the combined $(B - I)$ data (with the means, and linear trends subtracted for each night) is shown in Figure 3.

The strongest peak at $f = 9.7762 \pm 0.0001$ day $^{-1}$ exactly coincides with the beat period between the OP and LPP: $1/P_{beat} = 1/P_{orb} - 1/P_{phot}$, which was previously observed as the LSP and is the presumed precession period of the WD in FS Aur (Tovmassian, Zharikov, & Neustroev 2007). This $(B - I)$ data set is of sufficient length and photometric quality to compute an accurate, current ephemeris:

$$T_{B-I}(min) = 2455582.124(1) + 0.1022865(9) \cdot E \quad (3)$$

where $T_{B-I}(min)$ is the moment of the $(B - I)$ colour index minimum that corresponds to the hardest spectrum. Figure 10 (left panel) shows the $(B - I)$ phase curve folded according to the ephemeris (3) and averaged in 20 phase bins.

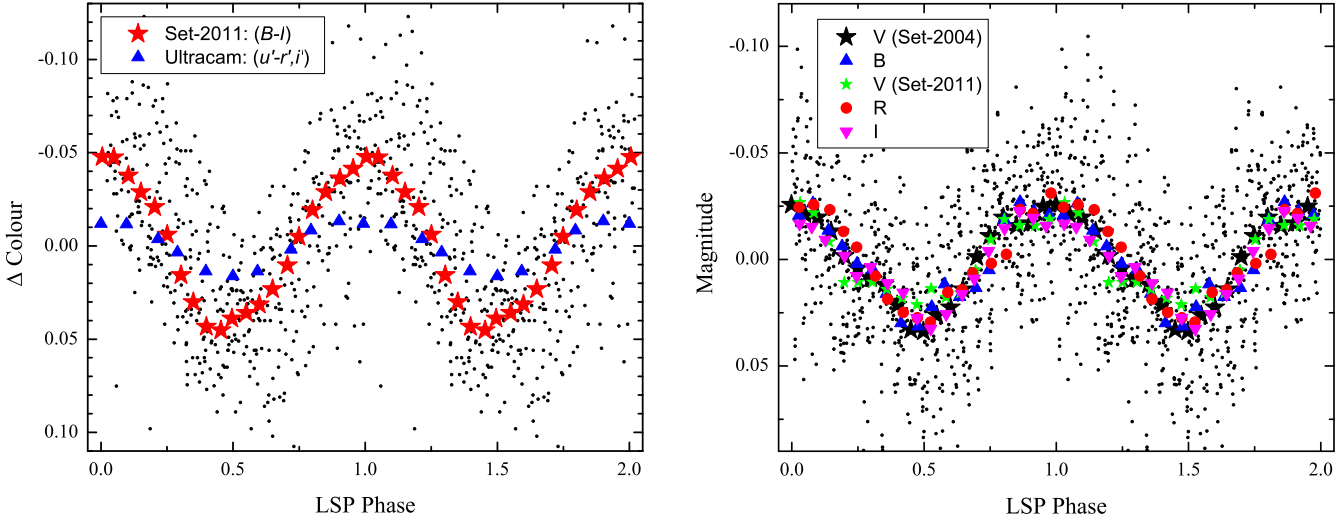


Figure 10. *Left:* The $(B - I)$ colour data of FS Aur (with the means, and linear trends subtracted for each night of observations) folded according to the ephemeris (4). The large red stars represent the $(B - I)$ data averaged in 20 phase bins. The blue triangles represent the Ultracam data folded according to the same ephemeris and averaged in 10 phase bins. *Right:* the folded light curves in different colours. The small dots represent the pre-whitened V data from the *set-2004* whereas the large black stars show the same data averaged in 20 phase bins. The other colour symbols represent the selected colour light curves of the *set-2011*. All data are plotted twice for continuity.

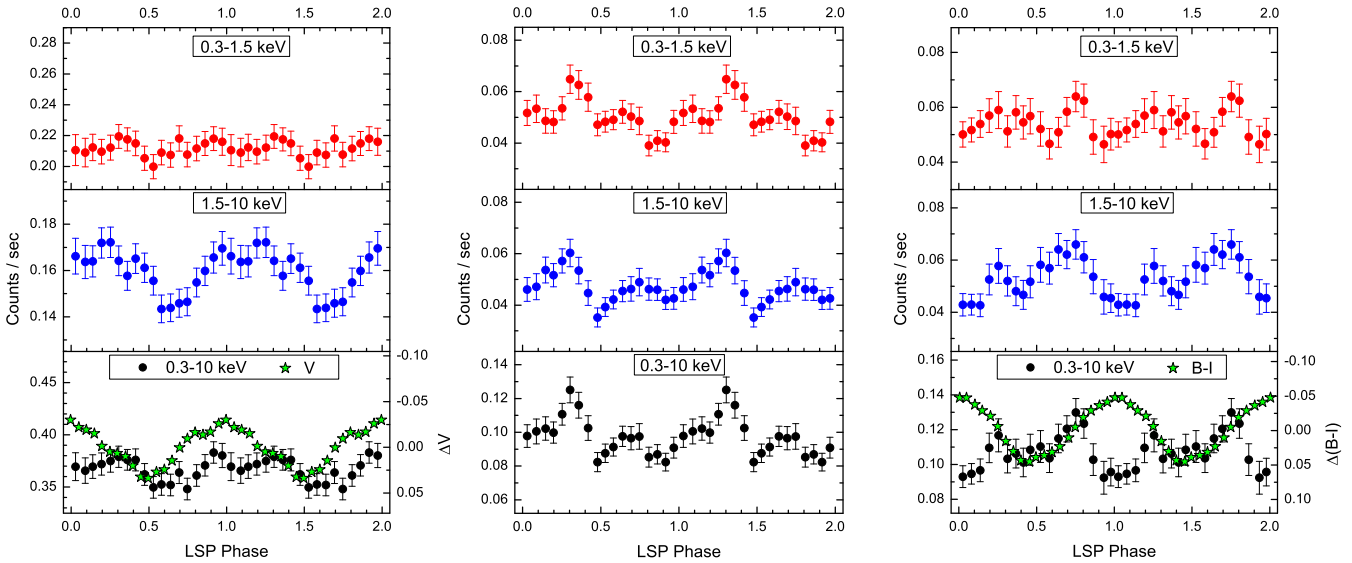


Figure 11. The Chandra (left panel), Swift-2007 (middle) and Swift-2011 (right) data folded with the LSP period according to the ephemeris (4). The panels are from top to bottom: the soft (0.3-1.5 keV), hard range (1.5-10 keV), and the total X-ray flux (0.3-10 keV). The latter are shown together with the corresponding colour or light curves (the Chandra data are compared with the optical pre-whitened V light curve from the *set-2004* whereas the Swift-2011 is compared with $(B - I)$ from the *set-2011*). All data are plotted twice for continuity.

For the following analysis it is useful to determine whether and how this colour variability might be related to brightness and spectral variability, and we also need to adjust the ephemeris (3) to be adequate for the *set-2004*. Unfortunately, the LSP modulation is scarcely visible in the raw light curve, yet it was visually detectable in a few nights of both sets of observations. On at least two nights of the *set-2011* this modulation is clearly seen in all the filters. It is

also occasionally seen in lesser number of filters on other nights⁵ (see the right panel of Fig. 9).

It seems that the LSP pulse profiles are nearly sinusoidal in all colour bands, and they are in phase with each other and with the $(B - I)$ colour curve (Fig. 10). The power spectra of the combined “good” data also show the significant peak at the LSP frequency in all four colour bands. We admit, however, that the timing analysis of these few manually selected nights is somewhat speculative.

⁵ In this sense, the V light curve seems worse than others that may be because of its most complex shape.

We now switch to the timing analysis of the *set-2004* where it has more credibility. Flickering and the LPP and OP pulsations were very strong during that time, hiding other, possibly weak, modulations. Nevertheless, after pre-whitening with the LPP and OP signals the LSP modulation becomes apparent, particularly in the *set-05*. The Lomb-Scargle periodogram of the pre-whitened light curve shows the strongest peak at $f = 9.7770 \pm 0.0002 \text{ day}^{-1}$ (Figure 3). We define the following current ephemeris for the moments of the pulse maximum: $T(max) = 2453347.064(2) + 0.102281(7) \cdot E$.

Unfortunately, a direct comparison of these two data sets is ambiguous. Even the more precise ephemeris (3) may not be accurate enough to be valid over the time period of 7 years. Clearly, there is no cycle count ambiguity, but the ephemeris prediction may be inaccurate as much as few tenths of the LSP. To be more confident, we compared the *set-2004* with the more recent simultaneous multicolour observations taken with the high-speed camera ULTRACAM in late 2003 (Neustroev et al. 2005). The most prominent feature of this light curve is the LPP. This variability is evident in all filters. However, in both the $(u' - r')$ and $(u' - i')$ colour indices a modulation with a shorter period of nearly 0.1 day has appeared. Assuming that this variability has the same nature as observed in the *set-2011*, we fitted the combined ULTRACAM colour curve with a sine wave of the LSP period and obtained the corrected value for the reference epoch time of the colour index minimum $T_{u'-r',i'}(min) = 2452942.518 \pm 0.001$. This again suggests that the colour and light modulations are in phase with each other.

Thus, we assume that there is no time lag between the colour and light modulations. We combined the pre-whitened *set-2004* and both the colour curves together into one large dataset. Its Lomb-Scargle periodogram is shown in Figure 3 (the bottom black line). The sharpness and power of the LSP signal at $f = 9.77644 \pm 0.00004 \text{ day}^{-1}$ indicates a very high degree of coherence. Finally, we refined the ephemeris in order to be adequate for all our data:

$$T(max) = 2452942.417(2) + 0.102286657(82) \cdot E \quad (4)$$

where $T(max)$ is the time of the optical pulse maximum, or the colour index minimum. Figure 10 shows different sets of our data folded according to ephemeris (4).

In X-rays, the modulation with the LSP is also evident in each X-ray set (Fig. 11). There appears to be a clear signature of the energy dependence of this modulation as to be directly visible in the light curves, and as seen in the hardness ratio curves (Fig. 6). This dependence is most prominent in the Chandra data where the soft photon flux is nearly constant while the hard flux exhibits strong quasi-sinusoidal variations (Fig. 11, left panel).

There are significant differences in the X-ray light curves between different X-ray sets. Unlike the Chandra's nearly sinusoidal modulation, the Swift light curves display complex double-peaked profiles. We suspect, however, that the latter also are sine-like in shape but distorted by a depression around LSP zeroth phase. This depression is deep and wide in *Swift-2011*, narrower and shallower in *Swift-2007*, and is scarcely seen in the Chandra set. If this supposition is correct then the sinusoidal component in all the X-ray data sets is nearly in phase with the optical modulation.

We can now compare the relative phasing of the photometric and radial velocity modulations with the LSP. We have used our previous radial velocity measurements made with a double Gaussian separation of 1600 km s^{-1} (for details see Tovmassian, Zharikov, & Neustroev (2007)). The LSP component, appearing in the far wings of emission lines, has maximum blueshift at phase 0.74 ± 0.02 , according to ephemeris (4). Thus,

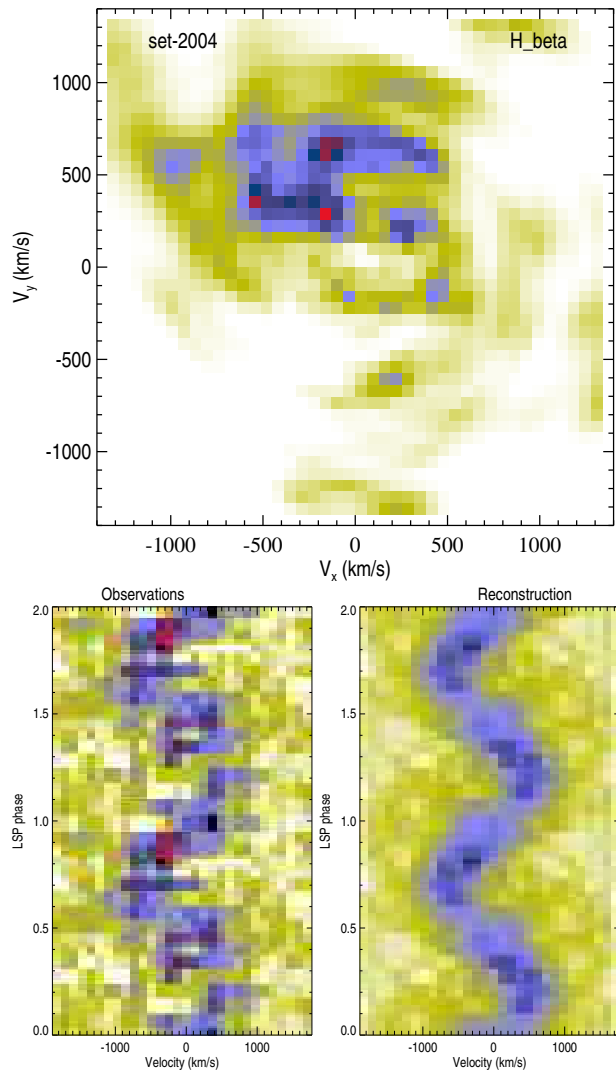


Figure 12. Doppler tomography for the $H\beta$ emission line from the *set-2004*. In the bottom panels are the line profile folded on the LSP cycle and then subtracted of the phase-invariant profile (left), and reconstructed profiles (right). In the top half the corresponding Doppler map is shown. For technical details see Hellier (1999).

it crosses the line of sight in front of the WD at the optical pulse maximum.

3.3.1 Doppler tomography of the LSP cycle of FS Aur.

In conclusion, we applied a Doppler imaging technique to calculate a tomogram on the LSP cycle of FS Aur. The original implementation of Doppler tomography has been used to map the emission regions in CVs using information stored in emission line profiles as a function of orbital phase (Marsh & Horne 1988). Such an approach allows to reconstruct the distribution of emission locked in the binary rest-frame, but other not orbital phase-locked emission components should they exist in the system, will be smeared out during the reconstruction. The latter case is common among the IPs which spectral lines often vary with additional to orbital periods, such as the spin period and its orbital sideband. In order to map the structures like the “accretion curtains” in IPs, one should calculate tomograms on the spin cycle. This technique has been

used, for example, by Hellier (1999) who showed that spin-cycle tomography is a useful diagnostic tool.

We found that it is instructive to apply a similar technique to image the LSP component of emission lines in FS Aur. We exactly followed the approach of Hellier (1999) and the interested reader should refer to this work for the technical details. The Doppler tomogram of the $H\beta$ emission line was calculated of 64 individual spectra obtained during two observing nights of Dec 8-9, 2004. The line profiles were folded on the LSP cycle, and then subtracted from the phase-invariant profile to leave only the LSP-varying component (Fig. 12, the bottom left panel). The spectra were phased according to ephemeris (4) thus phase 1 coincides with the optical pulse maximum. The resulting Doppler map is presented in the top panel of Fig. 12, whereas the reconstructed emission line profiles are shown in the bottom right panel of Fig. 12.

The LSP component produced the diffuse area of emission at 12 o'clock in the tomogram, the emission subtends $\sim 120^\circ$ at the origin. Its brightest part reaches $\sim 800 \text{ km s}^{-1}$, with a possible extension up to $\sim 1100 \text{ km s}^{-1}$ indicating that the source of the LSP emission is located close to the WD.

3.4 Searching for the spin period of the WD

A previous attempt to determine the spin period of the WD in FS Aur have proved inconclusive. Basing on high-speed photometric observations taken with ULTRACAM, Neustroev et al. (2005) reported the detection of oscillations with a period of ~ 101 and/or ~ 105 s associated with the spin period of the WD. Nevertheless, taking into account the short duration of those observations and the weakness of the detected signal, the authors suggested that new high signal-to-noise ratio observations of longer duration, and especially X-ray observations, would be very useful for confirming this unconvincing result.

From the presented data, the Chandra observations and the high time resolution data from the *set-2004* are the most suitable for the search for the spin period of the WD in FS Aur.

The Chandra light curve was extracted with a 22 s time resolution and has been Fourier analyzed to detect periodic signals. Inspection of the power spectrum at the high-frequency end (Fig. 13, left panel) reveals the strongest peak at 860.98 d^{-1} (100.35 ± 0.01 s). Even though this peak is still statistically insignificant, its frequency is very close to the one previously detected from the ULTRACAM photometry.

In order to probe if this signal is also present in the current optical data, we combined the observations obtained between JD 2453347–2453352 with the use of the telescopes located in South Korea, Italy and Mexico (Table 1). The Lomb–Scargle periodogram of this long data set with total exposure time of almost 87 hours is dominated (Fig. 13, left panel), at the higher frequencies, by a sharp and relatively strong peak which frequency is however different than that detected in the Chandra data: 847.218 d^{-1} (101.9808 ± 0.0001 s). To examine if this signal is real, we calculated the power spectra on individual nights and their parts. We found that the corresponding peak is present in all the power spectra except for the half-night of JD 2453352. Moreover, folding these subsets at the 101.9808-s period results in sinusoidal modulations of nearly identical amplitude of ~ 0.002 – 0.003 mag which are all in phase with each other (Fig. 13, right panel). All these indicate that the periodic 101.98-s modulation really exists. Nevertheless, its cause is still unclear.

If this is the spin period of the WD then we might expect to see the same modulation in X-rays, yet the Chandra power spectrum

shows no power at its frequency. On the other hand, the ~ 100.35 -s X-ray signal was occasionally clearly seen in the optical data. For example, in the periodogram of the night of JD 2453347 the 100.35-s peak is even stronger than the 101.98-s one (the dashed spectrum in the inset in Fig. 13, left panel). Furthermore, we call the reader's attention to the fact that the frequency difference of these two modulations is very close to the double LPP frequency, $2\omega_{LPP}$. This allows us to speculate that the real spin period is 100.35-s whereas the 101.98-s modulation is the optical $2\omega_{LPP}$ sideband.

In conclusion, we also evaluated for the short-term variability the *uvw2* and *uvm2* data from the *Swift-2007* observations which were taken in event mode. We found that the power spectrum of the *uvm2* data is again dominated by a number of peaks around 0.01 Hz. However, due to the extremely complex spectral window of the UVOT time-series, it is difficult to make a better conclusion on the exact frequency(ies) of dominated oscillation(s). We applied the CLEAN procedure (Roberts, Lehar, & Dreher 1987) to sort out the alias periods resulting from the uneven data sampling, but still obtained several strong peaks in this frequency region. Two of them, however, are located very close to the detected oscillations.

3.5 X-ray Spectral Analysis

Chavez et al. (2012) have recently shown that the optical brightness of FS Aur in quiescence varies within a wide range (17.4–15.2 mag). The Chandra observations reported in this paper were performed in the beginning of a significant decrease in luminosity. The Chandra data were taken when the optical brightness in *V* reached ~ 16.5 mag, ~ 0.8 mag weaker than observed few months earlier whereas during the Swift observations FS Aur was in the usual quiescent state and had the average brightness of $V=16.17$ in 2007 and $V=16.04$ in 2011. Interesting to note that the amplitude of variation of the average brightness in optical, UV and X-ray wavelengths is nearly the same. The UVOT photometry shows that during the Swift observations FS Aur had the average brightness of $UVW1=15.00$ and $UVW2=15.14$ in 2007 and $UVW1=14.84$ and $UVW2=15.03$ in 2011, with the corresponding X-ray count rate of 0.087 cts/s in 2007 and 0.098 cts/s in 2011. One can reasonably suspect that not only the X-ray flux, but also the X-ray spectrum might be variable, and thus simultaneous spectral fitting of all available data by a single model would not be feasible. Thus, we analyzed the Chandra and Swift spectra independently (because of the low count rate for each Swift observation, they were merged to improve the signal-to-noise ratio).

The X-ray spectrum of FS Aur can be characterized by a relatively smooth continuum with strong interstellar absorption that practically leaves no counts below 0.3 keV, and with several superimposed spectral lines, the most intense being the fluorescence Fe $K\alpha$ emission line at ~ 6.4 keV. The extracted spectra were fitted with XSPEC v12.7.1 (Arnaud 1996). The spectra were rebinned to have a minimum of 20 counts per bin to allow the use of the χ^2 -statistics.

The results of simple model fits, including single-component blackbody, thermal bremsstrahlung or collisionally ionized thermal equilibrium plasma models (BBODY, BREMS and MEKAL in XSPEC, respectively), along with a Gaussian to fit the Fe lines near 6.4 keV, have been shown to be inadequate to describe the spectrum, but multiple-temperature model fits are good. We found the best fits with composite models that consist of a combination of a number of MEKAL components with different temperatures but

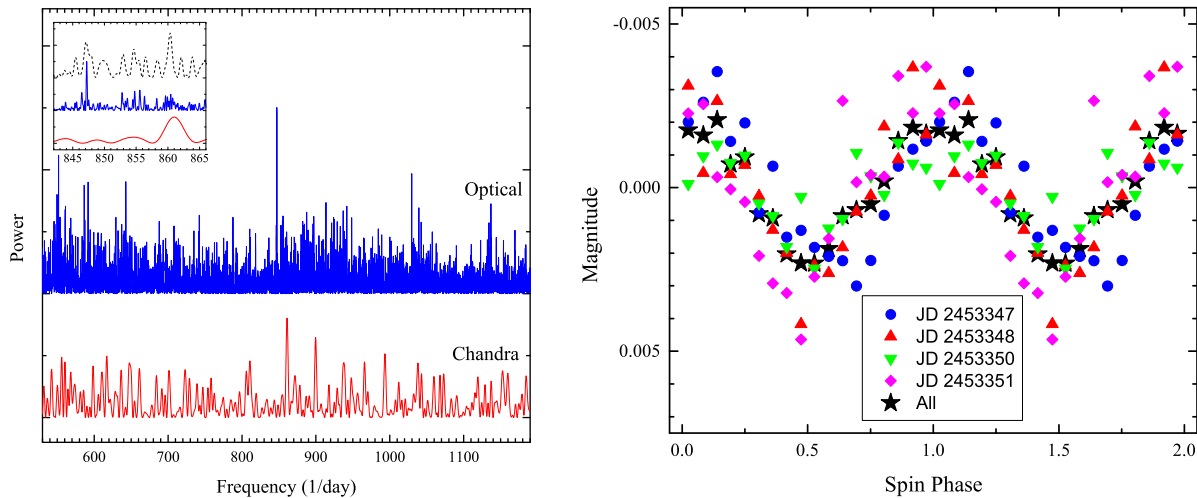


Figure 13. *Left panel:* The Lomb-Scargle power spectra for the Chandra data (red) and the high time resolution observations from the *set-2004* (blue). The frequency difference between the strongest peaks in these spectra at 860.98 d^{-1} (Chandra) and 847.218 d^{-1} (optical) is close to the double LPP frequency, $2\omega_{LPP}$. The inset shows the enlarged region around these frequencies. The dashed line represents the periodogram of the night of JD 2453347 in which both peaks are clearly seen. *Right panel:* The pre-whitened V light curves from the high time resolution observations obtained between JD 2453347–2453352, folded with the 101.98-s period. The large stars represent the entire data set, whereas the smaller symbols represent the individual nights. All data are plotted twice for continuity.

an identical abundance, absorbed by a partial covering absorption (PCFABS).

It is well known that in most IPs the spectra undergo strong photoelectric absorption which usually cannot be characterized by a single column density. Multiple absorption components are often required to adequately fit the spectra. We also tried using both simple photoelectric absorption (PHABS) and a partial covering absorber (PCFABS). We found, however, that there was no noticeable improvement with a multiple-absorber model, whereas a single partial covering absorber gave a slightly better result in most cases than a simple photoelectric absorber. We thus removed a simple absorber with no effect on the fit quality.

First the models were fitted to the strongest spectrum i.e. the averaged Chandra spectrum. The two-temperature MEKAL model with solar abundance (plus a Gaussian and absorption) gave a fit with $\chi^2_\nu = 1.13$ with temperatures 0.67 and 8.35 keV. The fit further improves ($\chi^2_\nu = 1.11$) when the metal abundance is left to free to vary. A third MEKAL component further improved the fit to $\chi^2_\nu = 1.04$. This fit gave temperatures of 0.64, 1.68 and 11.8 keV. The inclusion of additional MEKAL components gave a negligible improvement in χ^2 , so we show the parameters of the best-fit three-temperature MEKAL model in Table 4.

Even though a good fit to this averaged Chandra spectrum was obtained, the detected X-ray energy-dependent orbital variability of FS Aur (Section 3.1) suggests the distinct spectral variations over the orbital period. In order to investigate it further we extracted the pulsed and unpulsed spectra. The former was extracted for the orbital phase interval 0.27–0.43, approximately centered on the orbital spikes, the data from the time interval of the missing pulse were also included in this spectrum. The unpulsed spectrum consists the rest of the data. The count-rates of the pulsed and unpulsed spectra differ notably: 0.42 and 0.37 counts s^{-1} , respectively.

The unpulsed spectrum can be well fitted with the three-temperature MEKAL model, giving $\chi^2_\nu = 0.98$ with temperatures 0.64, 1.45 and 13.7 keV (we fixed the metal abundance at a value of 0.69). Even though the pulsed spectrum consists of only 1581 counts and suffers from their deficiency in the hardest ($\gtrsim 8$ keV)

and softest ($\lesssim 0.5$ keV) energies, it looks very similar to the unpulsed spectrum, yet it shows a notable flux excess in the 0.8–2.5 keV energy range. This spectrum was fitted with the same model in which we fixed the hardest MEKAL component temperature at the value determined for the unpulsed spectrum (13.7 keV). The fit gave $\chi^2_\nu = 0.92$ with the same temperature for the softest MEKAL component (0.63 keV) whereas the second MEKAL component has a higher temperature of 2.40 keV and a much larger normalization than for the unpulsed spectrum. The pulsed and unpulsed spectra together with the best fit model for the unpulsed spectrum and the residuals are shown in Fig. 14 (left panel).

The Swift averaged spectrum, when fitted with the same three-temperature MEKAL model, gives fit parameters very similar to those obtained for the Chandra data. We notice, however, that this model was not able to reproduce the iron $K\alpha$ emission line at 6.4 keV in the Swift spectrum, a separate Gaussian line (GAUSS) was required. The fit gave $\chi^2_\nu = 0.92$ with temperatures 0.52, 1.63 and 12.3 keV. The averaged Swift and Chandra spectra with the best fit models are shown in Fig. 14 (right panel).

The unabsorbed flux determined from the spectra in the 0.3–10 keV range was $4.34 \times 10^{-12} \text{ erg cm}^{-2} \text{ s}^{-1}$ during the Swift observations, ~ 40 per cent larger than during the Chandra observation ($3.22 \times 10^{-12} \text{ erg cm}^{-2} \text{ s}^{-1}$). This ratio is also kept in shorter energy subranges along the X-ray spectrum as well as in the optical band. Thus, despite the different states in which we found FS Aur during the Chandra and Swift observations, the shape of its spectrum from optical to X-rays shows little variations.

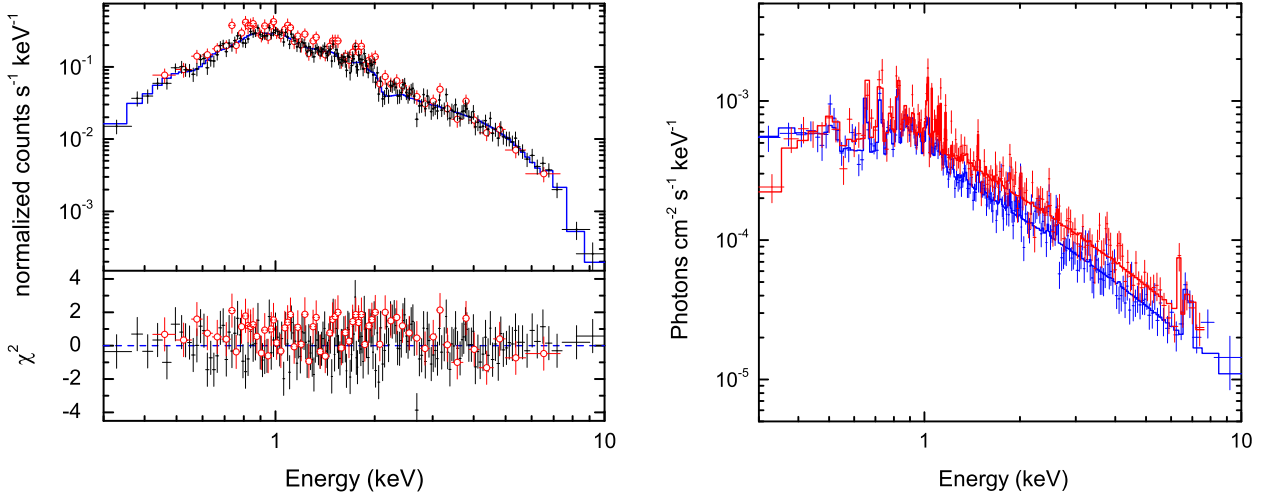
4 DISCUSSION

4.1 FS Aur as an Intermediate Polar

Since the first detailed investigations, FS Aur immediately attracted attention for having the very coherent, long periods (LPP and LSP) which exceed the orbital period. In order to explain such a discrepancy between the periods in FS Aur,

Table 4. Model components and parameters fitted to the phase-averaged spectrum of FS Aur. The errors are given to the same power of ten as the values.

Component	Parameter (Units)	Chandra (average)	Chandra (unpulsed)	Chandra (pulsed)	Swift
Part. Absn.	$N_{\text{H}} (\times 10^{21} \text{ cm}^{-2})$	$1.70_{-0.63}^{+1.05}$	$1.55_{-0.26}^{+0.36}$	$10.19_{-2.74}^{+2.50}$	$1.11_{-0.12}^{+0.12}$
	CvrFract	$0.70_{-0.08}^{+0.15}$	$0.70_{-0.05}^{+0.09}$	$0.75_{-0.07}^{+0.05}$	1.0 (frozen)
Mekal	kT (keV)	$0.64_{-0.05}^{+0.03}$	$0.64_{-0.06}^{+0.03}$	$0.63_{-0.05}^{+0.05}$	$0.52_{-0.07}^{+0.10}$
	Abundance	$0.69_{-0.20}^{+0.23}$	0.69 (frozen)	0.69 (frozen)	$0.34_{-0.22}^{+0.22}$
Mekal	Norm ($\times 10^{-3}$)	$0.15_{-0.04}^{+0.07}$	$0.14_{-0.02}^{+0.02}$	$0.59_{-0.20}^{+0.24}$	$0.12_{-0.02}^{+0.02}$
	kT (keV)	$1.68_{-0.40}^{+0.55}$	$1.45_{-0.27}^{+0.62}$	$2.40_{-0.38}^{+1.16}$	$1.63_{-0.29}^{+0.33}$
Mekal	Norm ($\times 10^{-3}$)	$0.20_{-0.09}^{+0.14}$	$0.16_{-0.05}^{+0.16}$	$2.12_{-0.57}^{+0.66}$	$0.30_{-0.11}^{+0.13}$
	kT (keV)	$11.8_{-2.14}^{+3.5}$	$13.7_{-2.6}^{+7.7}$	13.7 (frozen)	$12.3_{-2.6}^{+5.3}$
Mekal	Norm ($\times 10^{-3}$)	$1.54_{-0.12}^{+0.10}$	$1.54_{-0.10}^{+0.05}$	$0.76_{-0.71}^{+0.44}$	$2.23_{-0.14}^{+0.15}$
	χ^2_{ν} (dof)	1.04 (190)	0.98 (178)	0.92 (60)	0.92 (165)
Flux (obs), 0.3-10 keV ($\text{erg cm}^{-2} \text{ s}^{-1}$)		3.22×10^{-12}	3.2×10^{-12}	3.2×10^{-12}	4.34×10^{-12}

**Figure 14.** *Left panel:* The Chandra unpulsed (blue) and pulsed (red) spectra of FS Aur together with the best fit model for the unpulsed spectrum. The bottom panel shows the residuals. The pulsed spectrum shows an excess of counts, most notable in the 0.5–2.0 keV band. *Right panel:* The averaged Chandra (blue) and Swift (red) spectra with the best fit models. The flux determined from the Swift spectrum is ~ 40 per cent larger than determined from the Chandra spectrum.

Tovmassian, Zharikov, & Neustroev (2007) proposed the IP scenario with a rapidly rotating magnetic WD precessing with the LSP. The period of precession depends on the star parameters such as mass, size, shape, and the dynamics of its interior. According to existing models (Leins et al. 1992), the precession period of a WD is proportional to the third power of the spin period. In a slowly rotating compact star, the precession period is extremely long. However, in a rapidly rotating WD the precession period can explain observed long periodicities. In order to have the proposed precession period, the WD in FS Aur should be a fast rotator with the spin period of the order of 50-100 sec, according to calculations of Leins et al. (1992).

Because of the magnetic nature of the WD, one could expect to observe a strong and stable modulation in the X-ray and optical light curves with such a period. This hypothesis has received an observation confirmation after our detection of the ~ 100 s modulations in both the optical and X-ray data of FS Aur, even though the detected signal is rather weak, especially in X-rays. In this context, it is interesting to note that V455 And, another cataclysmic variable with many similar to FS Aur properties

(Tovmassian, Zharikov, & Neustroev 2007), has also been proven to possess a rapidly rotating WD with the spin period of 67.6 s (Gänsicke 2007; Bloemen et al. 2013). Similarly to FS Aur, the spin period of the WD in V455 And was found through extensive optical observations whereas the power at the spin frequency in X-rays is very low (Tovmassian, Zharikov, & Neustroev 2012).

This is slightly confusing but not really surprising. It was shown that if the magnetic and rotational axes of a WD are closely aligned, then spin modulations might be undetectable (Ramsay et al. 2008). Nevertheless, if such a WD in addition experiences a precession then another modulation with the precession period may appear. Other specific observational manifestations of precession are still to be understood. We guess, however, that as the primary reason for the temporal and spectral variability of the IPs with the spin period is the variable geometrical factor due to the sweeping around of the X-ray beam, a binary system with a precessing WD should share most of the observational properties with ordinary IPs and even might be virtually indistinguishable from them. On the whole, the closer the magnetic and rotational axes of a precessing WD are aligned, the more similarities such a binary

will share with a classical IP. The difference will only be apparent in the time scales of the variability: instead of modulations with the *spin and orbital-spin-beat* periods we expect to observe modulations with the *precession and orbital-precession-beat* periods. We believe that FS Aur is such a case.

Before discussing the nature of FS Aur in more detail, we briefly summarize the key observational properties of FS Aur which are relevant in this context:

(i) It has been proven that FS Aur exhibits a stable modulation in the optical and X-ray light curves with a period that is different from an orbital one (LSP).

(ii) The emission lines also vary with this period.

(iii) The optical light curve is normally dominated by variations at the beat period between the OP and the LSP: $1/P_{LPP} = 1/P_{OP} - 1/P_{LSP}$.

(iv) FS Aur is a rather hard X-ray source with low-energy absorption and the presence of Fe K α emission.

(v) Stockman et al. (1992) reported the detection of a non-zero circular polarization in FS Aur.

As seen, these properties of FS Aur satisfies most of Patterson's conditions for being an IP (Patterson 1994). They conflict only in the sense that in the canonical model of the IPs a period of optical and X-ray modulations due to the WD rotation is expected to be shorter than the OP. Nevertheless, as it was shown before, this restriction can be overtaken if a role of the WD rotation is played by the precession. One additional X-ray property of the IPs which was proposed by Norton, Watson, & King (1991) and which is also fulfilled by FS Aur – the presence of strong Fe K α emission. Furthermore, the small amplitude outbursts observed in FS Aur, are another good argument in favor of a truncated accretion disk in the system, i.e. the IP nature of FS Aur.

We now proceed to compare other properties of FS Aur such as the phasing of the optical and X-ray LSP pulses and their energy dependence with other well-studied IPs.

4.2 Comparison with other IPs

The spin period modulation is unambiguously detected in all the confirmed IPs as this is the defining characteristic of the class. This modulation is a direct consequence of the magnetically confined accretion flow onto the magnetic poles of the WD whose magnetic field is of sufficient strength to disrupt the accretion disc and to control the flow before it reaches the surface of the star. At some distance from the WD surface, the infalling material undergoes a strong shock, releasing X-rays as it cools by thermal bremsstrahlung and Compton cooling processes. Thus, it is widely supposed that the X-ray modulation reflects this physical process most clearly whereas the optical range is heavily affected by X-ray reprocessing. This, however, is not always the case. For example, DQ Her – the prototype of the subclass of IPs – is characterized by a very low X-ray flux and the strong spin modulation in the optical band.

IPs show a large variety of photometric and spectroscopic behaviour, both in X-rays and the optical range. In X-rays, for example, some IPs show a single-peaked pulsation whereas others show a double-peaked pulsation. There is also observed a strong dependence on the photon energy (usually, increasing modulation depth with decreasing energy).

The optical spin modulation, if observed, is usually correlated with the X-ray one. However, the optical variability is caused by the

reprocessing of variable X-ray irradiation that often resulted in significant sideband modulations. These sidebands and spin modulations can also have a strong wavelength-dependence. Furthermore, these modulations are observed not only in continuum but also in the hydrogen and He II emission lines. In many IPs the spin component, appearing in the far wings of the emission lines, has maximum blueshift near optical and/or X-ray pulse maximum (Hellier 1999).

Despite such complex behaviour, our understanding of IPs is now quite good. Most observable properties can be understood within the context of the widely accepted accretion curtain model (Rosen, Mason, & Cordova 1988; Hellier, Cropper, & Mason 1991). In this model, the material flows towards the magnetic poles of the WD in an arc-shaped curtain, and the largest X-ray and optical flux is seen when the upper pole is on the far side of the WD. It is not our intention to assess the strong and weak aspects of the model. Instead, we aim to compare the key, most reliable observable properties of FS Aur with those of the “ironclad” IPs. First of all, we pay attention to the optical brightness and colour variability with a spin period, and a mutual phasing between them and the emission line spin variability.

Unfortunately, such a comparison is not a simple task. Despite numerous multicolour observations of IPs conducted and published in the past, there are very few reports on the analysis of the colour spin variability. However, our primary result – the detection of the LSP variability through photometric observations – was obtained by means of the analysis of colour indices. Besides this variability being most confidently seen specifically in ($B - I$), our analysis also revealed another interesting property of the FS Aur colour time-series – its power spectrum is exclusively dominated by a peak at the LSP with no power at the LPP and the OP. We intended to test if the IPs show similar power spectra with the strongest peak at the spin frequency.

In order to conduct such an analysis, we requested our colleagues worldwide to provide us with their multicolour light curves. We were generously given the data of eight ironclad and confirmed IPs which show prominent spin modulations in the optical wavelengths alongside with different sidebands. Most of these observations were already published: PQ Gem (Hellier, Ramseyer, & Jablonski 1994), V405 Aur (Allan et al. 1996), NY Lup and IGRJ1509–6649 (Potter et al. 2012), DQ Her (Butters et al. 2009), EX Hya (Belle et al. 2005), FO Aqr (Chiappetti et al. 1989). Observations of AO Psc were obtained by E. L. Robinson and were extracted, alongside with Chiappetti et al.'s data of FO Aqr, from the collection of light curves of Albert Bruch (Fritz & Bruch 1998).

An analysis of all these data was performed in a similar fashion. We calculated the power spectra of the light and different colour curves, and then compared the light and colour curves folded with the spin period. Because of space limitations, we do not show any plots here⁶ but only give our conclusion on this study. We found that in *all* the IPs the power spectrum of the ($B - I$) or similar colour curve is dominated by a peak at the spin period with little power at the beats, in spite of the fact that in several systems the sideband variability is more prominent in the optical light curve than the spin modulation. As for energy dependence and phasing of the spin pulses in different wavelengths, they have not appeared to be very consistent even for these ironclad IPs.

In conclusion, and as an example of the most extreme case, we

⁶ See <http://vitaly.neustroev.net/research/intermediate-polars/ip-colours/> on each star for power spectra and pulse profiles.

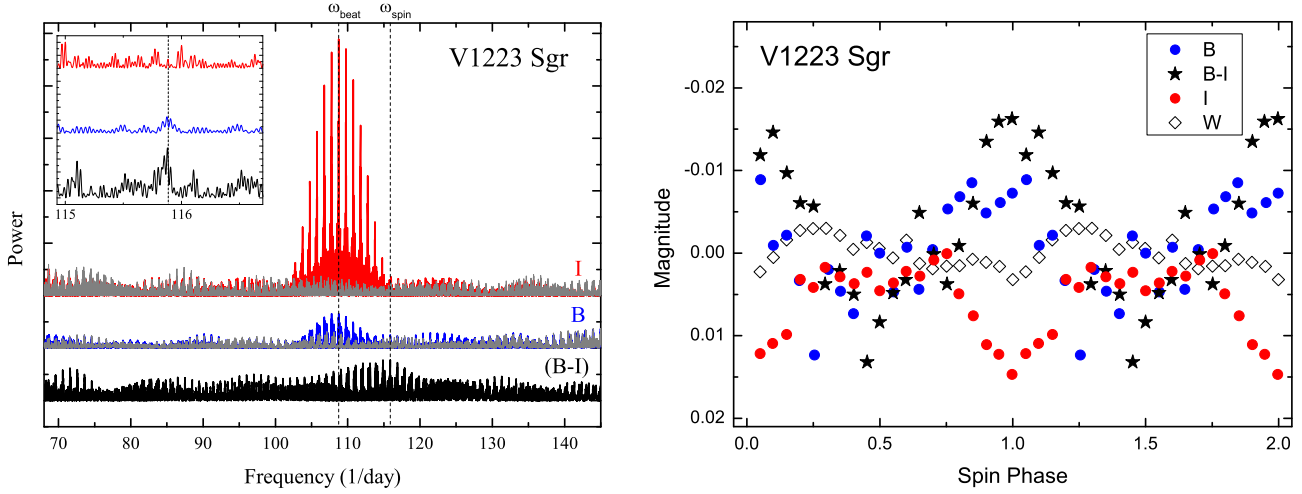


Figure 15. *Left panel:* The Lomb-Scargle power spectra of the B (blue) and I (red) light curves and the $(B - I)$ colour-index curve (black) of V1223 Sgr. The gray lines atop of the B and I periodograms represent corresponding pre-whitened spectra after the removal of the orbital frequency and the pulsation at the sideband frequency of 108.76 d^{-1} . The inset shows enlarged region around the spin frequency. *Right panel:* The B , I and unfiltered (white) light curves and the $(B - I)$ colour curve of V1223 Sgr folded with the spin period. All data are plotted twice for continuity.

present more detailed analysis of V1223 Sgr. This well-known IP is known to show very strong sideband modulations, whereas the spin pulsation is not seen in the optical. In this sense, the behaviour of V1223 Sgr is similar to FS Aur. Our own observations were used for the analysis.

Finally, we also performed an analysis of multicolour observations of V455 And which shows solid evidence for being an IP (Bloemen et al. 2013).

4.2.1 V1223 Sgr

V1223 Sgr has an orbital period of 3.37 h and a spin period of 745.6 s. The sinusoidal spin modulation dominates in X-rays and shows the increasing depth with decreasing energy. In the optical, however, the object pulsates at the 794.4 s sideband and no pulsations have been found at the spin period.

During 29 nights of September-October 2011 and 25 nights of May-June 2012 we conducted time-resolved observations of V1223 Sgr using the same telescope and equipment as for the observations of FS Aur. The observations of 2011 were done in unfiltered light and with an integration time of 45 sec. Most observations of 2012 were made with the B and I_c filters and with exposure times of 70 and 30 sec respectively. A detailed analysis of these data will be discussed elsewhere, here we concentrate on the variability with the spin period.

The 794.4 s sideband modulation was very strong in both filters. The power spectrum of the light curve is dominated by peaks at the sideband and orbital frequencies (108.76 and 7.13 day^{-1} respectively) with no (in I) or negligibly little power (in B) at the expected spin frequency $\Omega + \omega_{beat} = 115.89 \text{ day}^{-1}$ (Fig. 15, left panel). The latter modulation has not become apparent even in the pre-whitened light curve. However, in the power spectrum of the $(B - I)$ colour-index curve a peak emerges at the exact spin frequency. Folding the $(B - I)$ data over the spin period results in the nearly sinusoidal modulation with the amplitude of $\sim 0.03 \text{ mag}$ (Fig. 15, right panel). The folded B and I data also show a sign of pulsations even though the latter are very weak in power spectra. It is interesting that the character of such variability is very different from what we detected in other IPs. During around a half of the

spin period the B and I fluxes keep a nearly constant level, and then it increases in B and decreases in I . No pulsation is seen in the folded unfiltered light curve.

4.2.2 V455 Andromedae

V455 And (HS 2331+3905) is a high-inclination eclipsing dwarf nova. The system shares many similar properties with FS Aur and is known to show a variety of periodic photometric and spectroscopic variabilities. Araujo-Betancor et al. (2005) reported that V455 And exhibits two very different spectral periods, a short one of 81 min at the center and a longer one of 210 min in the wings of its emission lines. Eclipses in the system's light curve allowed an accurate and unambiguous determination of the orbital period of 81.08 minutes. However, the strongest peak in the photometric periodogram was located at twice the orbital frequency of 35.52 d^{-1} (40.54 min), while no power was detected at the orbital frequency of 17.76 d^{-1} even though a strong signal was found at 17.27 d^{-1} (83.38 min) and the one-day aliases (see Fig. 6 in Araujo-Betancor et al. 2005). Araujo-Betancor et al. interpreted it by a double-hump structure of the orbital light curve and the presence of permanent superhumps. Besides the orbital variability, V455 And exhibits a number of other periodic photometric variations and is proved to contain a magnetic WD. The 67.6 s spin period of the WD defines this object as an IP (Gänsicke 2007; Bloemen et al. 2013).

Nevertheless, similarly to FS Aur, the LSP ($\sim 3.5 \text{ h}$) appearing in the far wings of the emission lines, is not seen in the light curve of V455 And. Also, by analogy with FS Aur, one can expect to observe the LPP – photometric modulations with the beat period between the two spectral ones ($\sim 11 \text{ d}^{-1}$). Araujo-Betancor et al. did not mention any variability with such a period, even though their periodogram showed a marginal peak in this frequency region (Fig. 6 in their paper).

For analysis of the longer-term variability, during 11 nights of September 2011 we conducted BVR_cI_c time-resolved observations of V455 And using the same telescope and equipment as for the observations of FS Aur. A sample V light curve and $(B - V)$, $(V - R)$, $(R - I)$ and $(B - I)$ colour curves are shown in Figure 16 (left panel) while the Lomb-Scargle power spectra of the B , V , R , I

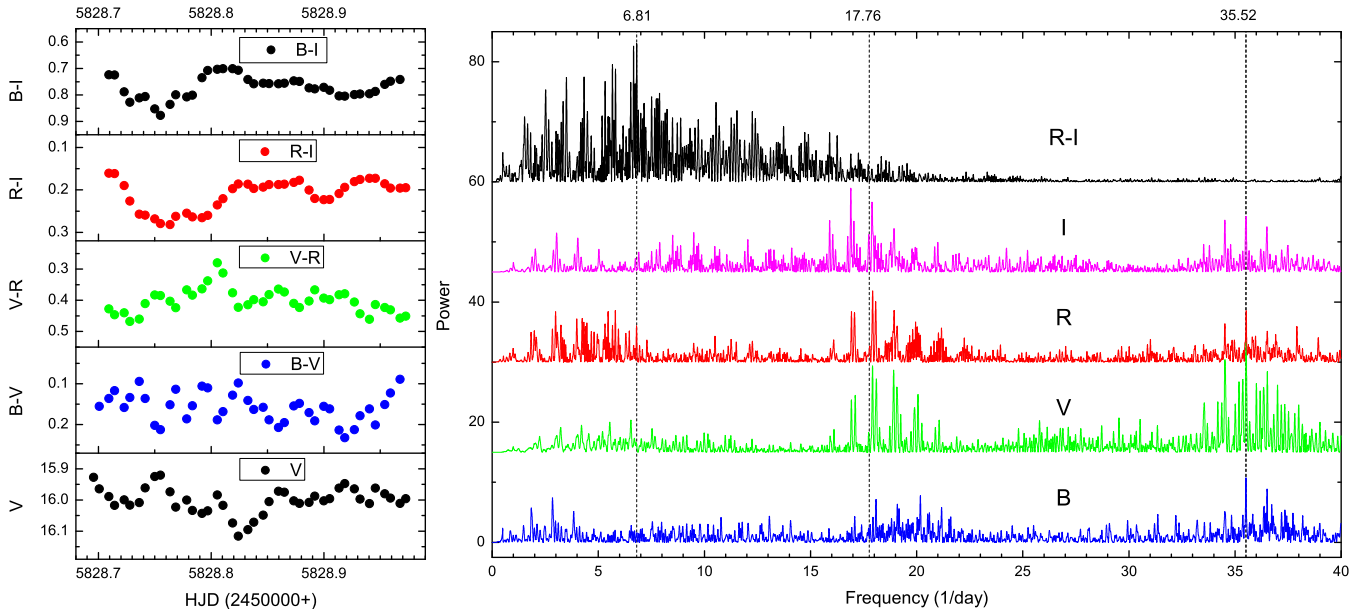


Figure 16. *Left panel:* Sample V light curve and $(B - V)$, $(V - R)$, $(R - I)$ and $(B - I)$ colour curves of V455 And from JD 2455 828. *Right panel:* The Lomb-Scargle power spectra of the $B V R I$ light curves and the $(R - I)$ colour-index curve of V455 And. No signal is detected at the orbital frequency of 17.76 d^{-1} but a strong signal is found at twice the orbital frequency of 35.52 d^{-1} . The $(R - I)$ periodogram shows excess of power in the low-frequency range with the strongest peaks at 6.81 d^{-1} and 6.62 d^{-1} . These frequencies are close to the spectroscopic period found from the radial velocity variations of the Balmer emission line wings (Araujo-Betancor et al. 2005; Tovmassian, Zharikov, & Neustroev 2007).

light curves and the $(R - I)$ colour-index curve are shown in the right panel of Figure 16 (from bottom to top of the figure).

The light curves and the $(B - V)$ and $(V - R)$ colour curves display periodic variability with a period of ~ 80 min. When folded with the orbital period, the double-hump structure of the light curves is clearly seen (not shown). The individual power spectra look similar to that presented by Araujo-Betancor et al. even though they are different in some details: a) the strengths of the strongest peaks at 35.52 d^{-1} and around the orbital frequency are now compatible (the 35.52 d^{-1} is stronger in the B band and weaker in I_c); b) the “superhump” peaks at 17.27 and 16.27 d^{-1} disappeared but new ones appeared at 16.93 and 17.1 d^{-1} and 17.93 and 18.1 d^{-1} .

However, the behavior of the colour indices $(B - I)$ and $(R - I)$ suggests a longer variability timescale. The corresponding periodograms show excess of power in the low-frequency range with the strongest peaks at 6.81 d^{-1} and 6.62 d^{-1} (211 min and 218 min) (better seen in $(R - I)$, Fig. 16). These frequencies are close to the spectroscopic period found from the radial velocity variations of the Balmer emission line wings (Araujo-Betancor et al. 2005; Tovmassian, Zharikov, & Neustroev 2007). We have to note that the power spectrum around these signals is complex, suggesting a lower degree of coherence.

This is not much of a surprise as despite the many similarities between V455 And and FS Aur, there is a fundamental difference between them. In the case of FS Aur, the long periods are very strict. For V455 And where only the LSP is reported, this period fluctuates on time scales of a few days (Araujo-Betancor et al. 2005; Tovmassian, Zharikov, & Neustroev 2007).

4.3 FS Aur and IPs: similarities and differences

The above analysis of multicolour optical light curves of well-known IPs has revealed a common property of the corresponding colour power spectra – the latter are dominated by a peak at the spin frequency even though the sideband variability is more prominent in the light curve than the spin modulation. The example of V1223 Sgr is the most notable, in which the $(B - I)$ power spectrum indicates the presence of the spin pulsation which is not seen in the optical light curve at all. This closely resembles the optical variability of FS Aur and V455 And with the LSP.

This effect can be naturally explained as a consequence of reprocessing of spin-modulated X-rays by asymmetric features in the system that are locked in the rotating binary frame, such as the secondary star or the bright spot (Hassall et al. 1981; Patterson & Price 1981). The photometric modulation appears due to the variation in the visible area of the reprocessing site which has a weak energy dependence. As a result, the sideband modulations are not present in colour data.

Knowledge of the orbital, spin and sideband ephemerides allows the question of the site of reprocessing in the system to be examined. Using FS Aur’s ephemerides (1), (2) and (4), one can see that the LSP and LPP modulations have coincident maxima at orbital phase 0.50 ± 0.01 . This corresponds to superior conjunction of the secondary and is likely due to heating of the inner hemisphere of the donor star that is quite typical among the IPs.

Nevertheless, there is a not very common characteristic of FS Aur which is worth to be mentioned: the relative phasing of the photometric and radial velocity modulations with the LSP. In contrast to most IPs, in which the spin component appearing in emission line wings has maximum blueshift near optical pulse maximum – phase 0 (Hellier 1999), in FS Aur the LSP component has maximum blueshift near phase 0.75. The latter results

in counter-clockwise rotation of the corresponding Doppler map (Fig. 12) though otherwise it closely resembles those of AO Psc and FO Aqr (Hellier 1999). The location of the emission area at "3 o'clock" in the IP tomograms and the occurring of maximum blueshift at phase 0 agree well with the accretion curtain model of IPs (Hellier, Cropper, & Mason 1991). The different spectral phasing of the LSP modulation in FS Aur indicates that instead of seeing a radiating gas flowing down the magnetic field lines on to the surface of the WD, as follows from the accretion curtain model, in FS Aur we observe a segment of the innermost region of the accretion disc moving with the local Keplerian velocity. This disagreement should not be considered a surprise if we admit that in fact the LSP is not the rotational period of the WD but the precession one. In this case the radial velocity variations with the short spin period must be smeared out during the LSP. However, a spin-averaged X-ray beam from FS Aur's WD would illuminate different segments of the accretion disc when sweeping around with the precession (LSP) period. These segments can reprocess high-energy emission into the optical and should have the Keplerian velocities. Thus the velocity modulation with the LSP would be phased with zero velocity at optical maximum, as it is observed in FS Aur (Fig. 17).

The LSP-folded trailed spectra and the corresponding Doppler map (Fig. 12) allow the location of this emission source to be estimated. The brightest part of the emission LSP-component reaches $\sim 800 \text{ km s}^{-1}$, with a possible extension up to $\sim 1100 \text{ km s}^{-1}$ (we note, however, that this higher velocity diffuse emission part of the tomogram might be an artefact of the reconstruction). Assuming Keplerian motion and adopting the system parameters given in Neustroev (2002), it implies a radial distance from the WD of $8 \times 10^9 \text{ cm}$ (~ 8 WD radii), with a possible extension inwards to about $4 \times 10^9 \text{ cm}$ (~ 4 WD radii). We suppose that this is a characteristic distance at which the accretion disc of FS Aur is disrupted by the magnetic field of the WD. It is somewhat shorter than supposed by the standard picture of IPs (~ 10 WD radii). On the other hand, IPs with shorter spin periods have smaller magnetospheres in which case the accretion discs are disrupted closer to the WD.

5 SUMMARY AND CONCLUSIONS

We have presented a comprehensive study of FS Aur based on two extensive sets of optical photometric observations and three X-ray data sets.

In addition to the formerly observed LPP and OP variations, these optical observations revealed, for the first time in photometric data, the presence of the LSP modulation, previously seen only spectroscopically. The LSP which is the presumed precession period of the WD, is best seen in the $(B - I)$ colour index derived from the 2010-2011 multicolour observations but it was also detected in the pre-whitened light curve from the 2004-2005 observational campaign. The analysis of X-ray observations made with Chandra and Swift, also revealed the existence of both the OP, LPP and LSP modulations.

We compared most reliable observable properties of the LSP pulsation such as energy dependence and phasing of the LSP pulses in different wavelengths, with those of the spin modulation of ten ironclad and confirmed IPs. We have found strong indications that the LSP signal detected in FS Aur's X-rays and optical photometry and spectroscopy is similar in nature to the spin modulation of the IPs. We conclude that even though some of observational properties of FS Aur are not very common, they are by no means unique to IPs. The most serious discrepancy is the relative phasing

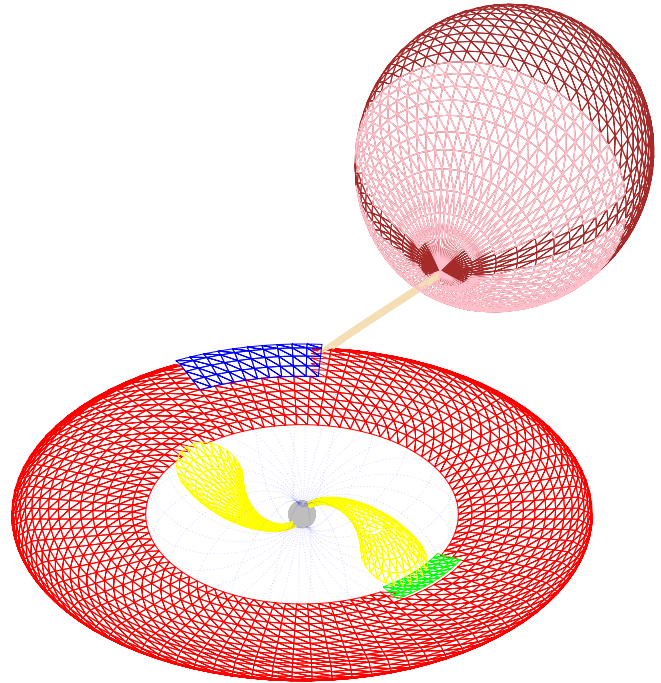


Figure 17. A schematic representation of the suggested geometry and components for FS Aur. The magnetic field of the WD disrupts the inner accretion disc and forces the accreting material to flow along field lines onto magnetic poles, forming arc-shaped, azimuthally extended accretion curtains. The spin component of the emission lines observed in an ordinary IP originates in a radiating gas which flows along the curtains (yellow) and has the radial infall velocity. In FS Aur, however, the radial velocity variations with the short spin period are smeared out during the LSP. Instead, a spin-averaged X-ray beam from FS Aur's WD illuminates different segments of the accretion disc when sweeping around with the precession (LSP) period. These segments (green) reprocess high-energy emission into the optical and have the Keplerian velocity. It crosses the line of sight in front of the WD at the optical LSP pulse maximum when the upper precessional pole points to the observer. The inner hemisphere of the secondary is the most probable candidate for being both the source of the orbital modulation and the reprocessing site of the sideband, LPP modulation.

of the photometric and radial velocity modulations with the LSP. In FS Aur the LSP spectral component has zero velocity at optical maximum, and it supports the precessional origin of the LSP variability (Figure 17).

In conclusion, we would like to mention a methodological aspect of this work. There is a long lasting discussion about a necessity of multicolour observations of CVs rather than unfiltered or single-filtered ones. Indeed, most time-resolved observations of variable stars nowadays are taken with relatively small telescopes, and the use of several filters is often considered as losing photons and wasting time. However, our analysis of multicolour observations of IPs has shown that time-series analysis of colour indices appears to be a powerful technique for revealing hidden variabilities and shedding light on their nature. For example, the $(B - I)$ power spectrum of V1223 Sgr indicates the presence in the data of the spin pulsation which is not seen in the optical light curve at all. Also, the analysis of the colour indices of V455 And revealed the presence in the photometrical data of the LSP pulsation which, similarly to FS Aur, was previously observed only spectroscopically. Our analysis has shown that the use of colour indices of bands

more distant in the spectrum, e.g. $(B - I)$, can be more efficient. We note that the $(B - I)$ colour index is a more sensitive estimator of the effective stellar temperatures with respect to the widely used $(B - V)$ (Natali et al. 1994).

ACKNOWLEDGMENTS

The authors thank Seathrún Ó Tuairisg, Caoilfhionn Lane, Genady Valyavin, Byeong-Cheol Lee and the staff of the Bohyunsan Optical Astronomy Observatory (BOAO) for assisting with the observations in 2004, Mike Rice and the staff at New Mexico Skies for their invaluable support, George B. and Elma Sjoberg who cared so much, and Natalia Neustroeva for help in the preparation of this paper. SZ and GT acknowledge PAPIIT grants IN-109209/IN-103912 and CONACyT grants 34521-E; 151858 for resources provided towards this research. Our research was based on X-ray observations by NASA missions Chandra and Swift which we acknowledge. We thank Neil Gehrels for approving the Target of Opportunity observation with Swift and the Swift team for executing the observation. This research has made use of data obtained through the High Energy Astrophysics Science Archive Research Center Online Service, provided by the NASA/Goddard Space Flight Center. We acknowledge photometric data kindly provided to us by our colleagues Kunegunda Belle, Albert Bruch, Oliver Butters, Jerry Foote, Boris Gänsicke, Coel Hellier, Keith Horne, Seppo Katajainen, Andrew J. Norton, Stephen Potter, Edward L. Robinson. We are thankful to the anonymous referee for careful reading of the manuscript.

REFERENCES

- Allan A., Horne K., Hellier C., Mukai K., Barwig H., Bennie P. J., Hilditch R. W., 1996, *MNRAS*, 279, 1345
- Araujo-Betancor S., et al., 2005, *A&A*, 430, 629
- Arnaud K. A., 1996, in *Astronomical Data Analysis Software and Systems V*, eds. Jacoby G. and Barnes J., ASP Conf. Series volume 101, 17
- Belle K. E., Howell S. B., Mukai K., Szkody P., Nishikida K., Ciardi D. R., Fried R. E., Oliver J. P., 2005, *AJ*, 129, 1985
- Berry R., Burnell J., 2005, *The handbook of astronomical image processing*, 2nd ed., Richmond, VA: Willmann-Bell
- Bloemen S., Steeghs D., De Smedt K., Vos J., Gänsicke B. T., Marsh T. R., Rodriguez-Gil P., 2013, *MNRAS*, 429, 3433
- Butters O. W., Norton A. J., Mukai K., Barlow E. J., 2009, *A&A*, 498, L17
- Chavez C. E., Tovmassian G., Aguilar L. A., Zharikov S., Henden A. A., 2012, *A&A*, 538, A122
- Chiappetti L., et al., 1989, *ApJ*, 342, 493
- Fritz T., Bruch A., 1998, *A&A*, 332, 586
- Gänsicke B. T., 2007, 15th European Workshop on White Dwarfs, 372, 597
- Gehrels N., et al., 2004, *ApJ*, 611, 1005
- Hassall B. J. M., et al., 1981, *MNRAS*, 197, 275
- Hellier C., 1996, in Evans A., Wood J. H., eds, *Astrophysics and Space Science Library*, Vol. 208, IAU Colloq. 158: Cataclysmic Variables and Related Objects. Kluwer, Dordrecht, p. 143
- Hellier C., 1999, *ApJ*, 519, 324
- Hellier C., Cropper M., Mason K. O., 1991, *MNRAS*, 248, 233
- Hellier C., Ramseyer T. F., Jablonski F. J., 1994, *MNRAS*, 271, L25
- Henden A. A., Honeycutt R. K., 1997, *PASP*, 109, 441
- Hoffmeister C., 1949, *Veroff. Sternw. Sonneberg* 1, 3
- Honeycutt R. K., Schlegel E. M., Kaitchuck R. H., 1987, *ApJS*, 65, 451
- King A. R., Lasota J.-P., 1991, *ApJ*, 378, 674
- Leins M., Soffel M. H., Lay W., Ruder H., 1992, *A&A*, 261, 658
- Marsh T. R., Horne K., 1988, *MNRAS*, 235, 269
- Misselt K. A., 1996, *PASP*, 108, 146
- Natali F., Natali G., Pompei E., Pedichini F., 1994, *A&A*, 289, 756
- Neustroev V. V., 2002, *A&A*, 382, 974
- Neustroev V. V., Zharikov S., Tovmassian G., Shearer A., 2005, *MNRAS*, 362, 1472
- Neustroev V., et al., 2012, *IAU Symposium*, 282, 79
- Norton A. J., Watson M. G., King A. R., 1991, *Lecture Notes in Physics*, 385, 155
- Norton A. J., Wynn G. A., Somerscales R. V., 2004, *ApJ*, 614, 349
- Potter S. B., Romero-Colmenero E., Kotze M., Zietsman E., Butters O. W., Pekeur N., Buckley D. A. H., 2012, *MNRAS*, 420, 2596
- Patterson J., 1994, *PASP*, 106, 209
- Patterson J., 2011, *Bulletin of the American Astronomical Society*, #103.03
- Patterson J., Price C. M., 1981, *ApJ*, 243, L83
- Poole T. S., et al., 2008, *MNRAS*, 383, 627
- Ramsay G., Wheatley P. J., Norton A. J., Hakala P., Baskill D., 2008, *MNRAS*, 387, 1157
- Roberts D. H., Lehar J., Dreher J. W., 1987, *AJ*, 93, 968
- Rosen S. R., Mason K. O., Cordova F. A., 1988, *MNRAS*, 231, 549
- Thorstensen J.R., Patterson J.O., Shambrook A., Thomas G., 1996, *PASP*, 108, 73
- Tovmassian G., et al., 2003, *PASP*, 115, 725
- Stockman, H. S., Schmidt, G. D., Berriman, G., et al. 1992, *ApJ*, 401, 628
- Tovmassian G. H., Zharikov S. V., Neustroev V. V., 2007, *ApJ*, 655, 466
- Tovmassian G., Zharikov S., Neustroev V., 2012, in *The Golden Age of Cataclysmic Variables and Related Objects*, F. Giovannelli & L. Sabau-Graziati (eds.), *Mem. SAI*, 83, 713
- Warner B., 1986, *MNRAS*, 219, 347
- Warner, B., 1995, *Cataclysmic Variable Stars* (Cambridge Astrophysics Ser. 28; Cambridge: Cambridge Univ. Press)
- Warner B., Wickramasinghe D. T., 1991, *MNRAS*, 248, 370

This paper has been typeset from a $\text{\TeX}/\text{\LaTeX}$ file prepared by the author.